DESY 11-035

Improved stochastic estimation of quark propagation with Laplacian Heaviside smearing in lattice QCD

C. Morningstar,[1] J. Bulava,[2] J. Foley,[3] K.J. Juge,[4] D. Lenkner,[1] M. Peardon,[5] and C.H. Wong[1]

[1]*Department of Physics, Carnegie Mellon University, Pittsburgh, PA 15213, USA*
[2]*NIC, DESY, Platanenallee 6, D-15738, Zeuthen, Germany*
[3]*Dept. of Physics and Astronomy, University of Utah, Salt Lake City, UT 84112, USA*
[4]*Dept. of Physics, University of the Pacific, Stockton, CA 95211, USA*
[5]*School of Mathematics, Trinity College, Dublin 2, Ireland*

(Dated: April 19, 2011)

A new method of stochastically estimating the low-lying effects of quark propagation is proposed which allows accurate determinations of temporal correlations of single-hadron and multi-hadron operators in lattice QCD. The method is well suited for calculations in large volumes. Contributions involving quark propagation connecting hadron sink operators at the same final time can be handled in a straightforward manner, even for a large number of final time slices. The method exploits Laplacian Heaviside (LapH) smearing. Z_N noise is introduced in a novel way, and variance reduction is achieved using judiciously-chosen noise dilution projectors. The method is tested using isoscalar mesons in the scalar, pseudoscalar, and vector channels, and using the two-pion system of total isospin $I = 0, 1, 2$ on large anisotropic $24^3 \times 128$ lattices with spatial spacing $a_s \sim 0.12$ fm and temporal spacing $a_t \sim 0.034$ fm for pion masses $m_\pi \approx 390$ and 240 MeV.

PACS numbers: 12.38.Gc, 11.15.Ha, 12.39.Mk

I. INTRODUCTION

Recent discoveries of new hadronic resonances have generated much excitement in the field of hadron spectroscopy. The current surge in experimental activity underlines the need for a better understanding of excited hadronic states from the theory of quantum chromodynamics (QCD). Presently, Markov-chain Monte Carlo estimates of QCD path integrals defined on a space-time lattice offer the best way to make progress in this regard.

Calculating the mass spectrum of excited-state hadron resonances is a key goal in lattice QCD. However, such calculations are very challenging. Computational limitations cause simulations to be done with quark masses that are unphysically large, leading to pion masses that are heavier than observed and introducing systematic errors in all other hadron energies. The use of carefully designed quantum field operators is crucial for accurate determinations of low-lying energies. To study a particular state of interest, the energies of all states lying below that state must first be extracted, and as the pion gets lighter in lattice QCD simulations, more and more multi-hadron states lie below the masses of the excited resonances. The evaluation of correlations involving multi-hadron operators contains new challenges since not only must initial to final time quark propagation be included, but also final to final time quark propagation must be incorporated. The masses and widths of resonances (unstable hadrons) cannot be calculated directly in finite-volume Monte Carlo computations, but must be deduced from the discrete spectrum of finite-volume stationary states for a range of box sizes[1–4].

Our approach to constructing hadron operators appropriate for such calculations was outlined in Refs. [5, 6]. Our first study of the nucleon and Δ excitations in the quenched approximation was presented in Ref. [7], and nucleon results for two flavors of dynamical quarks appeared in Ref. [8]. A survey of excited-state energies in small volume for the isovector mesons and kaons using $N_f = 2 + 1$ dynamical quarks was given in Ref. [9], along with results for the Λ, Σ, Ξ baryons. Other recent progress in calculating excited-state energies in lattice QCD can be found in Refs. [10–15]. All of our results to date have been achieved in small volume with pions having masses comparable to or heavier than about 390 MeV. Our goal now is to extend our efforts into larger volumes and using lighter pions. To do this, the issue of multi-hadron states must be addressed.

In this work, we focus on the problem of incorporating multi-hadron operators into finite-volume excited-state spectrum calculations in lattice QCD. To compute the finite-volume stationary-state energies of QCD, one must first evaluate a matrix of temporal correlations $C_{ij}(t_F - t_0) = \langle 0 | T\, O_i(t_F)\, \overline{O}_j(t_0) \, | 0 \rangle$, where T denotes time-ordering, the source operators $\overline{O}_j(t_0)$ create the states of interest at an initial time t_0, and the sink operators $O_i(t_F)$ annihilate the states of interest at a later time t_F. The correlation functions $C_{ij}(t)$ can be expressed in terms of "path" integrals over quark $\overline{\psi}, \psi$ fields and gluon U fields involving the QCD action having the form

$$S[\overline{\psi}, \psi, U] = \overline{\psi} K[U] \psi + S_G[U], \tag{1}$$

where $K[U]$ is known as the Dirac matrix and $S_G[U]$ is the gauge-field action. Integration over the Grassmann-valued quark fields introduces a $\det K$ and factors of K^{-1} in the remaining integrals over the gluon U field, and when formulated on a Euclidean space-time lattice, such path integrals can be estimated using the Monte Carlo method with Markov-chain importance sampling. Incorporating the $\det K$ in the Monte Carlo updating and eval-

uating the elements of K^{-1} (the quark propagators) are the most computationally demanding parts of the calculations.

Once estimates of a Hermitian matrix of temporal correlation functions $C_{ij}(t)$ are obtained, several procedures for extracting the lowest stationary-state energies $E_0, E_1, E_2, \ldots$ in any given symmetry channel are available[16, 17]. For example, let $\lambda_n(t, t_0)$ denote the eigenvalues of the Hermitian matrix $C(t_0)^{-1/2}\, C(t)\, C(t_0)^{-1/2}$, where t_0 is some fixed reference time (typically small) and the eigenvalues, also known as the *principal* correlation functions, are ordered such that $\lambda_0 \geq \lambda_1 \geq \cdots$ as t becomes large. Then one can show that

$$\lim_{t\to\infty} \lambda_n(t, t_0) \;=\; e^{-E_n(t-t_0)}. \qquad (2)$$

Determinations of the principal correlators $\lambda_n(t, t_0)$ for sufficiently large temporal separations t yield the desired energies E_n.

The rows and columns of the gauge-covariant Dirac matrix $K[U]$ can be viewed as compound indices which incorporate the lattice space-time site indices and the quark color, flavor, and spin indices. Hence, K is a very large matrix, and determining and storing all of the elements of K^{-1} is not possible. Symmetries are used to eliminate the need to compute all K^{-1} elements. Computations are usually arranged such that the linear system of equations $Kx = y$ needs to be solved for only a manageable number of source vectors y. For temporal correlations of single-hadron operators (excluding isoscalar mesons), invariance under all spatial and temporal translations dramatically reduces the number of K^{-1} elements required. In such cases, the hadron creation operator needs to be considered only on one initial time slice and only at a single spatial site, yielding the so-called point-to-all method. A handful of points can be used to increase statistics.

To study a particular eigenstate, the procedure by which energies are extracted from Monte Carlo estimates of temporal correlation functions using Eq. (2) requires that all eigenstates lying below the state of interest must first be extracted. As the pion gets lighter in lattice QCD simulations, more and more *multi-hadron* states will lie below the excited resonances, and multi-hadron operators will be needed to accurately compute the energies of such states. For example, a good baryon-meson sink operator which annihilates a total zero momentum is typically a superposition of terms having the form

$$B(-\boldsymbol{p}, t)M(\boldsymbol{p}, t) = \frac{1}{V^2}\sum_{\boldsymbol{x},\boldsymbol{y}} \varphi_B(\boldsymbol{x}, t)\varphi_M(\boldsymbol{y}, t)e^{i\boldsymbol{p}\cdot(\boldsymbol{x}-\boldsymbol{y})},$$

where V is the spatial volume of the lattice, $2\boldsymbol{p}$ is the relative momentum, and $\varphi_B(\boldsymbol{x}, t)$ and $\varphi_M(\boldsymbol{y}, t)$ are appropriate localized interpolating fields for a baryon and a meson, respectively. In the evaluation of the temporal correlations of such a multi-hadron operator, it is not possible to completely remove all summations over the spatial sites on the source time slice using translation invariance. Hence, the need for estimates of the quark propagators K^{-1} from all spatial sites on a time slice to all spatial sites on another time slice cannot be sidestepped. Some correlators involve diagrams with quark lines originating at the sink time t_F and terminating at the same sink time t_F (see Fig. 1), so quark propagators involving a large number of quark-line starting times must also be handled.

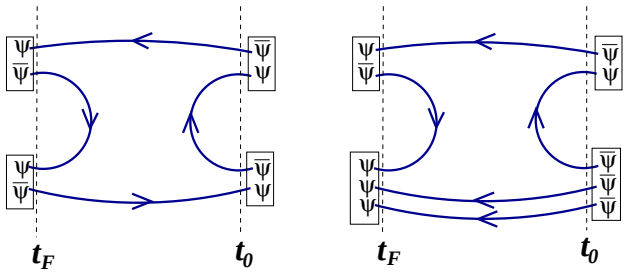

FIG. 1: Examples of quark-line diagrams in multi-hadron correlators involving the $\overline{\psi}$ field on the later time t_F connecting to a ψ field also on the later time slice t_F. The initial time is denoted by t_0. (Left) A two-meson correlator. (Right) The correlator of a baryon-meson system.

Finding better ways to incorporate the low-lying effects of such slice-to-slice quark propagation for large numbers of quark source times is crucial to the success of our excited-state hadron spectrum project at lighter pion masses. A new method, known as distillation[18], uses a novel quark-field smearing procedure that facilitates exact treatment of slice-to-slice quark propagation. Although distillation was found to work well, calculations with that method are costly, making it feasible only on small lattices. Here, we propose to combine the quark-field smearing used in Ref. [18] with a new stochastic approach to estimating the quark propagators, resulting in a much more efficient treatment suitable for large volumes. Describing and testing this new method is the aim of this work. This method was briefly introduced with preliminary testing in Refs. [9, 19, 20].

The remainder of this paper is organized as follows. The stochastic LapH method is described in Sec. II. Laplacian Heaviside quark-field smearing is reviewed, and our new stochastic treatment of quark propagation is detailed. The method involves Monte Carlo estimation of quark propagation using Z_N noise in the LapH subspace with variance reduction achieved through the introduction of suitable noise dilution projectors. The new method is compared to an earlier procedure which uses noise introduced on the space-time lattice itself. The number of inversions of the Dirac matrix needed in the new method is demonstrated to be insensitive to the volume of the lattice. Details on how the temporal correlations of hadron operators are evaluated using the stochastic LapH method are then presented in Sec. III. Full source-sink factorization is seen to be another advantageous feature of the method, especially for com-

putations of correlation matrices involving large sets of hadron operators. Various implementation details are given in Sec. IV. Applications of the method to the isoscalar mesons in the scalar, pseudoscalar, and vector channels and to the two-pion system of total isospin $I = 0, 1, 2$ using anisotropic $24^3 \times 128$ lattices with pion masses $m_\pi \approx 390$ and 240 MeV are then presented in Sec. V. Conclusions are summarized in Sec. VI.

II. DESCRIPTION OF THE METHOD

The use of smeared fields is crucial for successfully extracting the spectrum of QCD in our Monte Carlo computations. Hadron operators constructed out of smeared fields have dramatically reduced mixings with the high-frequency modes of the theory that obscure the low-lying eigenstates of interest. Our operators are constructed using spatially-smoothed link variables $\widetilde{U}_j(x)$ and spatially-smeared quark fields $\widetilde{\psi}(x)$.

The spatial links are smeared using the stout-link procedure described in Ref. [21]. Note that only spatial staples are used in the link smoothening; no temporal staples are used, and the temporal link variables are not smeared.

The quark field for each quark flavor is smeared using

$$\widetilde{\psi}_{a\alpha}(x) = \mathcal{S}_{ab}(x,y)\ \psi_{b\alpha}(y), \tag{3}$$

where x, y are lattice sites, a, b are color indices, α is a Dirac spin component, and the smearing kernel $\mathcal{S}$ is such that the smeared field behaves in exactly the same way as the original field under all time-independent symmetry transformations on a cubic lattice. For extracting energies from temporal correlations, it is important that only spatial smearing is used. In other words, the smearing kernel is diagonal in time: $\mathcal{S}_{ab}(x,y) \propto \delta_{x_4 y_4}$. In addition, our smearing kernel is independent of spin.

We use the new Laplacian Heaviside (LapH) quark-field smearing scheme which has been described in Ref. [18] and is defined by

$$\mathcal{S} = \Theta\left(\sigma_s^2 + \widetilde{\Delta}\right), \tag{4}$$

where $\widetilde{\Delta}$ is the three-dimensional gauge-covariant Laplacian defined in terms of the stout-smeared gauge field $\widetilde{U}$, and σ_s is the smearing cutoff parameter. The Laplacian matrix is given by

$$\widetilde{\Delta}^{ab}(x,y;U) = \sum_{k=1}^{3}\Big\{\widetilde{U}_k^{ab}(x)\delta(y,x+\hat{k}) + \widetilde{U}_k^{ba}(y)^*\delta(y,x-\hat{k}) - 2\delta(x,y)\delta^{ab}\Big\}, \tag{5}$$

where x, y are lattice sites, and a, b are color indices. This is a Hermitian matrix which is block-diagonal in time. It is important to use the stout-smeared gauge links when smearing the quark field since doing so dramatically reduces the statistical errors in the correlations of the hadron operators we use which involve covariantly-displaced quark fields[8]. The gauge-covariant Laplacian operator is ideal for smearing the quark field since it is one of the simplest operators that locally averages the field in such a way that all relevant symmetry transformation properties of the original field are preserved.

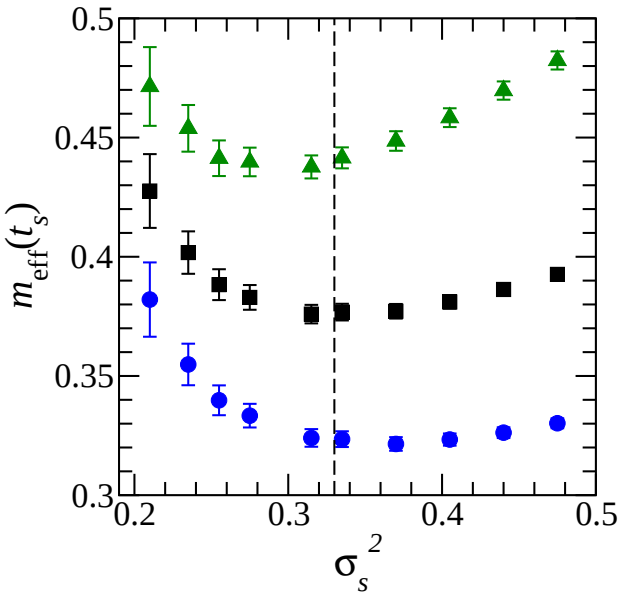

FIG. 2: The effective masses for temporal separation $t_s = 1$ for three representative nucleon operators against the LapH smearing cutoff σ_s^2. Results were obtained using $N_f = 2 + 1$ configurations on a $16^3 \times 128$ anisotropic lattice with spacing $a_s \sim 0.12$ fm for stout-link smearing with $n_\xi = 10$ iterations and staple weight $\xi = 0.1$. The circles show results (shifted downward by 0.04) for a single-site operator. The squares correspond to a singly-displaced nucleon operator, and the triangles are the results (shifted upward by 0.04) for a triply-displaced-T operator. The value $\sigma_s^2 \approx 0.33$ is observed to be a good choice.

Let V_Δ denote the unitary matrix whose columns are the eigenvectors of $\widetilde{\Delta}$, and let Λ_Δ denote a diagonal matrix whose elements are the eigenvalues of $\widetilde{\Delta}$ such that

$$\widetilde{\Delta} = V_\Delta\ \Lambda_\Delta\ V_\Delta^\dagger. \tag{6}$$

The LapH smearing matrix is then given by

$$\mathcal{S} = V_\Delta\ \Theta\left(\sigma_s^2 + \Lambda_\Delta\right)\ V_\Delta^\dagger. \tag{7}$$

All of the eigenvalues in Λ_Δ are real and less than zero. Hence, the matrix $\Theta(\sigma_s^2 + \Lambda_\Delta)$ has unit entries on those diagonal elements corresponding to eigenvalues whose magnitudes are less than σ_s^2 and zero entries for all other elements. Given that $\widetilde{\Delta}$ is block-diagonal in time, each eigenvector has nonzero elements only on one time slice, so we can associate any given eigenpair with that particular time. The eigenvalues of $\widetilde{\Delta}$ always occur such that approximately N_v eigenvalues have magnitude smaller than

σ_s^2 on each time slice. We have observed that the number of eigenvalues on each time slice that survive the Heaviside function varies from time to time by only one or two in cases where N_v exceeds sixty or more. Hence, the Heaviside smearing matrix is well approximated by fixing N_v to the same value on each time slice and for each gauge configuration.

Let V_s denote the matrix whose columns are in one-to-one correspondence with the eigenvectors associated with the N_v lowest-lying eigenvalues of $-\widetilde{\Delta}$ on each time slice. Then our LapH smearing matrix is well approximated by the Hermitian matrix

$$\mathcal{S} = V_s \, V_s^\dagger. \tag{8}$$

This is the actual smearing matrix used in our calculations. Note that on a lattice having N_t time slices and N_s sites in each of the spatial directions, the matrix V_s has $N_v N_t$ columns and $N_t N_s^3 N_c$ rows, where $N_c = 3$ is the number of quark colors. The $N_v N_t$ eigenvectors that form the smearing matrix span the so-called LapH subspace.

To set the parameter σ_s, and hence N_v, several small simulations were done varying this parameter while computing the effective masses for a handful of simple meson and baryon operators. We chose the value of σ_s that minimized the effective masses at a chosen early time separation t_s. The effective masses for $t_s = 1$ for three representative nucleon operators are shown in Fig. 2 against values of σ_s. A single-site nucleon operator in which all three quark fields are taken at the same site is shown, as well as a singly-displaced nucleon operator in which one of the quarks is displaced away from the other, and a triply-displaced-T operator in which all three quarks are displaced from the others in a T configuration. The value $\sigma_s^2 \approx 0.33$ was chosen. This value is insensitive to which time interval is used as long as t_s is small enough such that contributions from excited states have not decayed away. It is also insensitive to the choice of hadron operator used and the quark mass. We expect σ_s to change little with the lattice spacing.

Evaluating the temporal correlations of our hadron operators requires combining matrix elements associated with various quark lines $\mathcal{Q}$. Since we construct our hadron operators out of covariantly-displaced, smeared quark fields, each and every quark line in our computation involves the following product of matrices:

$$\mathcal{Q} = D^{(j)} \mathcal{S} \Omega^{-1} \mathcal{S} D^{(k)\dagger}, \tag{9}$$

where $\Omega = \gamma_4 K$ and $D^{(i)}$ is a gauge-covariant displacement of type i. The displacement type can be trivial (no displacement), a displacement in a given single spatial direction on the lattice by some number of links (typically three), or a combination of two or more spatial lattice directions. The use of $\Omega = \gamma_4 K$ is convenient for ensuring baryon correlation matrices that are Hermitian.

An exact treatment of such a quark line is best accomplished by writing

$$\mathcal{Q} = D^{(j)} V_s \, (V_s^\dagger \Omega^{-1} V_s) \, V_s^\dagger D^{(k)\dagger}, \tag{10}$$

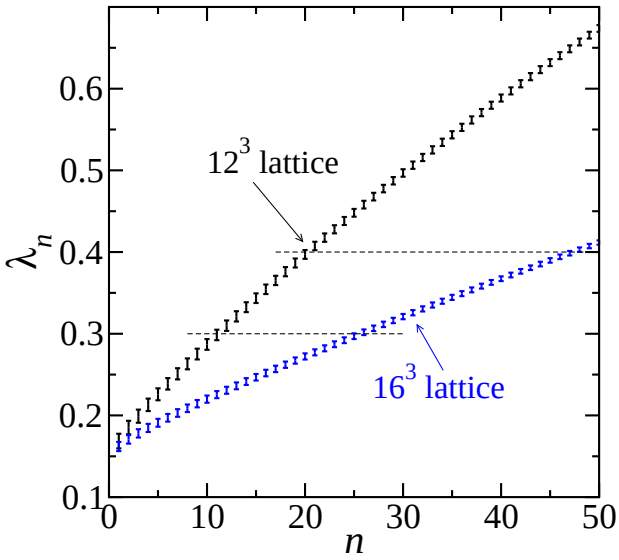

FIG. 3: The effect of the spatial lattice volume on the eigenvalues of the gauge-covariant Laplacian operator. λ_n is the n-th lowest eigenvalue of $-\widetilde{\Delta}$ on a given time slice. The error bars show the variation over different time slices and over a set of $N_f = 2 + 1$ configurations. The lattice spacings a_s are both near 0.12 fm, and the pion masses are both near 0.70 GeV. Link smearing with $n_\xi = 10$ iterations and staple weight $\xi = 0.1$ was used. For the 12^3 lattice, there are nine eigenvalues between 0.3 and 0.4, whereas for the 16^3 lattice, there are 22 eigenvalues between 0.3 and 0.4, demonstrating that the density of eigenvalues is proportional to the spatial volume of the lattice (at sufficiently high values). The lowest-lying modes do not change very much with the lattice volume.

then one needs to compute and store only the elements of the much smaller matrix $V_s^\dagger \Omega^{-1} V_s$ instead of computing and storing a very large number of Ω^{-1} elements. Let $N_d = 4$ denote the number of Dirac spin components, and define $y_{c\beta}^{(i,\alpha)}(x) = V_s(c, x;\ i)\ \delta_{\alpha\beta}$, where α, β are spin indices, c indicates color, x is a lattice site, and i refers to the column of V_s which is the i-th eigenvector of the Laplacian. Then solving the linear system $\Omega x = y^{(i,\alpha)}$ for x and all i, α by standard methods yields $\Omega^{-1} V_s^{(i)}$. Hence, $N_v N_t N_d$ such inversions are required in order to obtain the full matrix $V_s^\dagger \Omega^{-1} V_s$ for each quark mass and each gauge configuration in the Monte Carlo ensemble. If only one source time slice is used in the hadron correlators, then $N_v N_d$ inversions are required per quark mass per gauge configuration. Once multi-hadron operators are included, however, sink-to-sink quark lines are needed, so $N_v N_{\rm snk} N_d$ inversions must be done, where $N_{\rm snk}$ is the number of sink times. Generally, a handful of hadron source times are used to improve statistics, so upon including multi-hadron operators, one finds that the number of inversions needed in practice ends up near $N_v N_t N_d$.

Solving the linear systems $\Omega x = y$ is a major component of the computational cost of evaluating the hadron correlators once a Monte Carlo ensemble is generated.

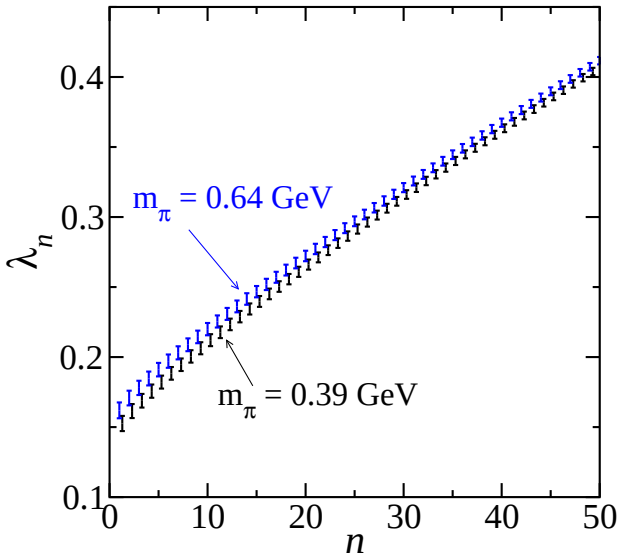

FIG. 4: The small effect of the light-quark mass on the eigenvalues of the gauge-covariant Laplacian operator. λ_n is the n-th lowest eigenvalue of $-\widetilde{\Delta}$ on a given time slice. The error bars show the variation over different time slices and over a set of $N_f = 2+1$ configurations on a $16^3 \times 128$ anisotropic lattice with $a_s \sim 0.12$ fm for link smearing $n_\xi = 10$ and $\xi = 0.1$.

It turns out that the number N_v of required eigenvectors on each time slice rises in direct proportion to the spatial volume of the lattice, as shown in Fig. 3. The number of eigenvectors is also fairly insensitive to the light quark mass, as shown in Fig. 4. Initial calculations on 16^3 lattices with spatial spacing $a_s \approx 0.12$ fm showed that $N_v = 32$ worked well. On 20^3 lattices, $N_v = 64$ was needed, and for the $24^3 \times 128$ lattices used in this study, we found that $N_v = 112$ levels were below the σ_s^2 cutoff. We have generated gauge configurations on $32^3 \times 256$ anisotropic lattices. On these lattices, we find that $N_v = 264$, so the number of inversions needed becomes $N_v N_t N_d > 270,000$ for each configuration and each quark mass, which is far too large to be feasible with current computing resources.

Fortunately, an exact treatment of the quark lines is not needed. In fact, we have found that exact treatment of the quark lines is very wasteful. Given our use of the Monte Carlo method to evaluate the path integrals over the gauge link variables, the statistical errors in our estimates of the hadron correlators are ultimately limited by the statistical fluctuations arising from the gauge-field sampling. Thus, we only need to estimate the quark lines to an accuracy comparable to the gauge noise from the Monte Carlo method. Such estimates can be obtained with far fewer inversions than required by an exact treatment of the quark lines.

Random noise vectors η which satisfy $E(\eta_i) = 0$ and $E(\eta_i \eta_j^*) = \delta_{ij}$, where $E()$ denotes an expected value as defined in probability theory, are useful for stochastically estimating the inverse of a large matrix Ω as follows. Assume that for each of N_R noise vectors, we can solve the following linear system of equations: $\Omega X^r = \eta^r$ for X^r, where r labels the noise vectors $r = 1, 2, \cdots, N_R$. Then $X^r = \Omega^{-1}\eta^r$, and $E(X_i \eta_j^*) = \Omega_{ij}^{-1}$ so that a Monte Carlo estimate of Ω_{ij}^{-1} is given by $\Omega_{ij}^{-1} \approx N_R^{-1} \sum_{r=1}^{N_R} X_i^r \eta_j^{r*}$. Unfortunately, this equation usually produces stochastic estimates with variances which are much too large to be useful. Variance reduction is done by *diluting* the noise vectors[22–24]. A given dilution scheme can be viewed as the application of a complete set of projection operators $P^{(b)}$. Define $\eta^{r[b]} = P^{(b)}\eta^r$, and define $X^{r[b]}$ as the solution of $\Omega X^{r[b]} = \eta^{r[b]}$, then a much better Monte Carlo estimate of Ω_{ij}^{-1} is

$$\Omega_{ij}^{-1} \approx \frac{1}{N_R} \sum_{r=1}^{N_R} \sum_b X_i^{r[b]} \eta_j^{r[b]*}. \tag{11}$$

The dilution projections ensure *exact zeros* for many of the $E(\eta_i \eta_j^*)$ elements instead of estimates that are only statistically zero, resulting in a dramatic reduction in the variance of the Ω^{-1} estimates. The use of Z_N noise ensures zero variance in our estimates of the diagonal elements $E(\eta_i \eta_i^*)$. The effectiveness of the variance reduction depends on the projectors chosen.

Earlier stochastic methods[25, 26] introduced noise in the full spin-color-space-time vector space, that is, on the entire lattice itself. However, since we intend to use Laplacian Heaviside quark-field smearing, an alternative is possible: noise vectors ρ can be introduced *only in the LapH subspace*. The noise vectors ρ now have spin, time, and Laplacian eigenmode number as their indices. Color and space indices get replaced by Laplacian eigenmode number. Again, each component of ρ is a random Z_N variable so that $E(\rho) = 0$ and $E(\rho\rho^\dagger) = I_d$, where I_d is the identity matrix. Dilution projectors $P^{(b)}$ are now matrices in the LapH subspace. In the stochastic LapH method, a quark line on a gauge configuration is evaluated as follows:

$$\begin{aligned}
\mathcal{Q} &= D^{(j)} \mathcal{S} \Omega^{-1} \mathcal{S} D^{(k)\dagger}, \\
&= D^{(j)} \mathcal{S} \Omega^{-1} V_s V_s^\dagger D^{(k)\dagger}, \\
&= \textstyle\sum_b D^{(j)} \mathcal{S} \Omega^{-1} V_s P^{(b)} P^{(b)\dagger} V_s^\dagger D^{(k)\dagger}, \\
&= \textstyle\sum_b D^{(j)} \mathcal{S} \Omega^{-1} V_s P^{(b)} E(\rho\rho^\dagger) P^{(b)\dagger} V_s^\dagger D^{(k)\dagger}, \\
&= \textstyle\sum_b E\Big(D^{(j)} \mathcal{S} \Omega^{-1} V_s P^{(b)} \rho \, (D^{(k)} V_s P^{(b)} \rho)^\dagger \Big).
\end{aligned} \tag{12}$$

Displaced-smeared-diluted quark source and quark sink vectors can be defined by

$$\varrho^{[b]}(\rho) = D^{(j)} V_s P^{(b)} \rho, \tag{13}$$

$$\varphi^{[b]}(\rho) = D^{(j)} \mathcal{S} \Omega^{-1} \, V_s P^{(b)} \rho, \tag{14}$$

and each quark line on a given gauge configuration can be estimated using

$$\mathcal{Q}_{uv}^{(AB)} \approx \frac{1}{N_R} \delta_{AB} \sum_{r=1}^{N_R} \sum_b \varphi_u^{[b]}(\rho^r) \; \varrho_v^{[b]}(\rho^r)^*, \tag{15}$$

where the subscripts u, v are compound indices combining space, time, color, spin, and quark displacement type, B is the flavor of the source field and A is the flavor of the sink field. The above quark line estimate has the form of an outer product expansion. Such estimates are frequently used in the compression of digital images, so the stochastic LapH estimate can be viewed as a lossy compression of the quark propagation.

Occasionally, it is useful to estimate a quark line using γ_5-Hermiticity to switch the source and sink. Using $K^\dagger = \gamma_5 K \gamma_5$, it is straightforward to see that another way to estimate a quark line is using

$$\mathcal{Q}_{uv}^{(AB)} \approx \frac{1}{N_R} \delta_{AB} \sum_{r=1}^{N_R} \sum_b \overline{\varrho}_u^{[b]}(\rho^r)\ \overline{\varphi}_v^{[b]}(\rho^r)^*, \qquad (16)$$

defining

$$\overline{\varrho}(\rho) = -\gamma_5\gamma_4 \varrho(\rho), \qquad \overline{\varphi}(\rho) = \gamma_5\gamma_4 \varphi(\rho). \qquad (17)$$

Eqs. (15) and (16) are meant to be used inside Monte Carlo estimates of path integrals over the gauge link variables. To simplify matters, the Monte Carlo within a Monte Carlo computation can be combined into a single larger Monte Carlo calculation over both gauge link variables and quark line noises, effectively setting $N_R = 1$ for each gauge configuration. However, each quark line in a hadron correlator needs an independent noise to ensure unbiased estimation. For example, a baryon correlator requires at least three noises per gauge configuration. Once inversions are done for a handful of such noise vectors for a given configuration, noise permutations can be used to increase statistics.

The dilution projectors we use are products of time dilution, spin dilution, and LapH eigenvector dilution projectors. The full projector index $b = (b_T, b_S, b_L)$ is a triplet of indices, where b_T is the time projector index, b_S is the spin projector index, and b_L is the LapH eigenvector projector index. Our noise-dilution projectors have the form

$$P^{(b)}_{t\alpha n;\ t'\alpha' n'} = P^{(b_T)}_{t;t'}\ P^{(b_S)}_{\alpha;\alpha'}\ P^{(b_L)}_{n;n'}, \qquad (18)$$

where t, t' refer to time slices, α, α' are Dirac spin indices, and n, n' are LapH eigenvector indices. For each type (time, spin, LapH eigenvector) of dilution, we studied four different dilution schemes. Let N denote the dimension of the space of the dilution type of interest. For time dilution, $N = N_t$ is the number of time slices on the lattice. For spin dilution, $N = 4$ is the number of Dirac spin components. For LapH eigenvector dilution, $N = N_v$ is the number of eigenvectors retained on each time slice. The four schemes we studied are defined below:

$$\begin{aligned}
P^{(b)}_{ij} &= \delta_{ij}, && b = 0, && \text{(no dilution)}\\
P^{(b)}_{ij} &= \delta_{ij}\ \delta_{bi}, && b = 0, \ldots, N-1 && \text{(full dilution)}\\
P^{(b)}_{ij} &= \delta_{ij}\ \delta_{b,\lfloor Ji/N \rfloor} && b = 0, \ldots, J-1, && \text{(block-}J\text{)}\\
P^{(b)}_{ij} &= \delta_{ij}\ \delta_{b,\, i \bmod J} && b = 0, \ldots, J-1, && \text{(interlace-}J\text{)}
\end{aligned}$$

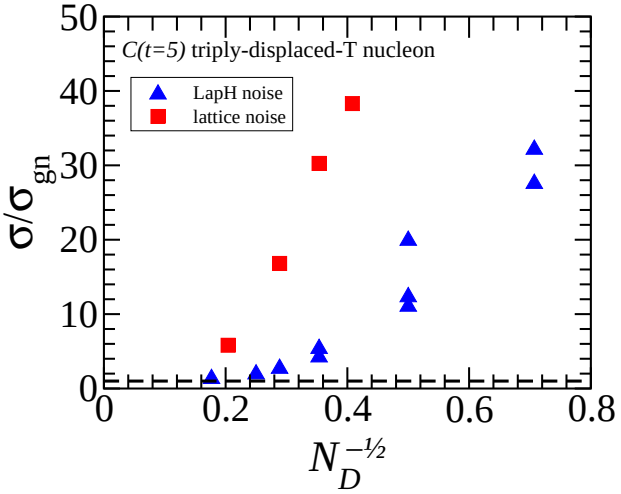

FIG. 5: Comparison of the new stochastic LapH method (triangles) with the earlier stochastic method using noise on the full lattice (squares) for the correlator $C(t = 5)$ of a triply-displaced-T nucleon operator on a $16^3 \times 128$ lattice. The vertical scale is the ratio of statistical error σ (with no averaging over the six permutations of the three noises) over the error in the gauge-noise limit $\sigma_{\rm gn}$, and in the horizontal scale, N_D is the number of Dirac-matrix inversions per source per quark line. Each point shows an error ratio using a particular dilution scheme. The LapH points lie significantly below the results from the lattice noise method, indicating a dramatic variance reduction.

where $i, j = 0, \ldots, N-1$, and we assume N/J is an integer. Note that each projector is a diagonal matrix with some or all of the diagonal elements set to unity and all other elements vanishing. We use a triplet (T, S, L) to specify a given dilution scheme, where "T" denote time, "S" denotes spin, and "L" denotes LapH eigenvector dilution. The schemes are denoted by 1 for no dilution, F for full dilution, and BJ and IJ for block-J and interlace-J, respectively. For example, full time and spin dilution with interlace-8 LapH eigenvector dilution is denoted by (TF, SF, LI8).

Introducing noise in this way produces correlation functions with significantly reduced variances, as shown in Fig. 5. Let $C(t)$ denote the correlation function of a representative triply-displaced-T nucleon operator at temporal separation t. Let $\sigma_{\rm gn}$ represent the statistical error in $C(t = 5)$ using exactly-determined slice-to-slice quark propagators. In other words, $\sigma_{\rm gn}$ arises solely from the statistical fluctuations in the gauge configurations themselves (the gauge noise limit). Let σ denote the error in $C(t = 5)$ using stochastic estimates of the quark propagators. The vertical axis in Fig. 5 is the ratio of the statistical error σ in $C(t = 5)$ over $\sigma_{\rm gn}$. Results are shown for a variety of different dilution schemes. In the lattice noise method, variance reduction is achieved with projectors which dilute in the time, spin, and color indices. Simple spatial dilutions are also used. The squares show results for dilution schemes with noise introduced in the larger spin-color-space-time vector space, and the

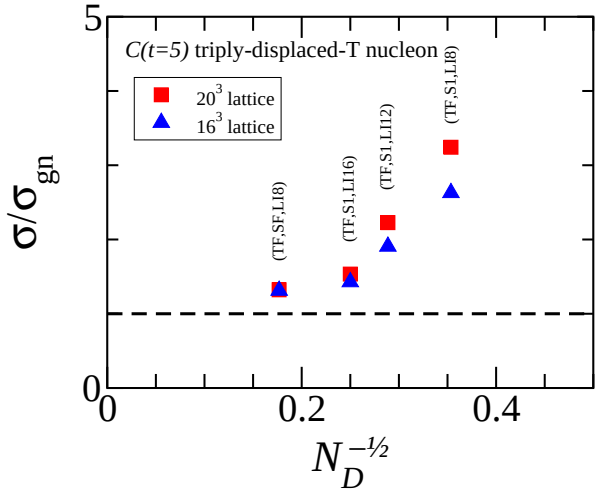

FIG. 6: Comparison of the new stochastic LapH method on 16^3 (triangles) and 20^3 (squares) lattices for the correlator $C(t = 5)$ of a triply-displaced-T nucleon operator on a $16^3 \times 128$ lattice. The vertical scale is the ratio of statistical error σ (with averaging over the six permutations of the three noises) over the error in the gauge-noise limit $\sigma_{\rm gn}$, and in the horizontal scale, N_D is the number of Dirac-matrix inversions per source per quark line. Each point shows an error ratio using a particular dilution scheme. The number of Laplacian eigenvectors needed is 32 on the 16^3 lattice and 64 on the 20^3 lattice. The leftmost points correspond to the dilution scheme (TF, SF, LI8). For this scheme, $\sigma/\sigma_{\rm gn} = 1.31$ on the 16^3 lattice and $\sigma/\sigma_{\rm gn} = 1.32$ on the 20^3 lattice.

triangles show results for different dilution schemes using noise introduced only in the LapH subspace. The triangles show nearly an order of magnitude reduction in the statistical error, compared to the square symbols. The correlator for other time separations t and for a variety of other hadron operators were also examined. All of the observables we studied showed the same dramatic reduction in the variance using the new LapH-noise method compared to the lattice-noise method.

The number of Dirac matrix inversions needed in the stochastic LapH method to achieve a target statistical precision was found to be insensitive to the spatial volume, despite the rapid increase in the number of LapH eigenvectors. Calculations on a 16^3 and a 20^3 lattice were carried out and the ratios $\sigma/\sigma_{\rm gn}$ for various correlators at various time separations were compared. The error ratios for the representative triply-displaced-T nucleon correlator for time separation $t = 5$ on a 16^3 lattice (triangles) are compared to those from a 20^3 lattice (squares) in Fig. 6. For the (TF, SF, LI8) dilution scheme, we found $\sigma/\sigma_{\rm gn} = 1.31$ for this quantity on the 16^3 lattice and $\sigma/\sigma_{\rm gn} = 1.32$ on the 20^3 lattice. Not only is the equality of these ratios on the two volumes remarkable, but also their closeness to unity is striking. Keep in mind that the number of Laplacian eigenvectors needed doubles in going from the smaller to the larger volume. These results show that once a sufficient number of dilution projectors are used, the number of inversions required by the stochastic LapH method does not increase with the lattice volume and are sufficient to essentially reach the gauge noise limit. Additional inversions of the Dirac matrix are totally unnecessary since they do not lower the error any further. Other time separations and a variety of other hadron operators were also studied and led to the same conclusions.

Different dilution schemes were explored using 16^3, 20^3, and 24^3 spatial lattices with spacing $a_s \sim 0.12$ fm and light quark masses yielding pion masses ranging from 240 MeV to 500 MeV, and we have found that the scheme (TF, SF, LI8) produces variances near that of the gauge noise limit for correlators which involve only quark lines that connect the source and sink time slices. Interlace-J and block-J were observed to work equally well for spin and LapH eigenvector dilutions. For correlators which involve quark lines that originate and terminate at the final sink time, the dilution scheme (TI16, SF, LI8) was found to work well. The interlacing in time enables us to evaluate quark lines that originate on *any* time slice. Results for several isoscalar correlators using (TI32, SF, LI8) on 20 configurations were compared with (TI16, SF, LI8) and no differences in the variances were discernible, suggesting the gauge noise limit has essentially been reached.

In the stochastic LapH method, the number of times that $\Omega x = y$ must be solved is $N_\rho N_P$ for each gauge-field configuration, where N_ρ is the number of Z_N noises used and N_P is the number of dilution projectors. Using full time dilution (with four choices of source time t_0), full spin dilution and interlace-8 LapH eigenvector dilution, then the t_0-to-t_F (for sink time t_F) quark lines require 128 inversions for each noise on each configuration. To accommodate a baryon-meson system, at least 5 noises for these quark lines are needed. The t_F-to-t_F quark lines use interlace-16 time dilution, full spin dilution, and interlace-8 LapH eigenvector dilution, requiring 512 inversions per noise per configuration. Two noises are required for these quark lines. Hence, a total of $5 \times 128 + 2 \times 512 = 1664$ inversions per configuration are needed to compute all baryons and mesons composed of u, d quarks. This number of inversions is the same for both the 24^3 and 32^3 lattices that we plan to use. An exact treatment of the quark propagation requires 57,344 inversions per configuration on $24^3 \times 128$ lattices for $N_v = 112$ and 270,336 inversions per configuration on $32^3 \times 256$ lattices for $N_v = 264$.

III. TEMPORAL CORRELATIONS OF HADRON OPERATORS

Details on how the temporal correlations of hadron operators are evaluated using the stochastic LapH method are presented in this section. We limit our attention to four cases: baryon to baryon, meson to meson, two-meson to meson, and two-meson to two-meson systems. Other source to sink cases are straightforward generalizations of the four examples below.

A. Baryon to baryon correlations

All of our hadrons are assemblages of basic building blocks which are covariantly-displaced, LapH-smeared quark fields:

$$q^A_{a\alpha j} = D^{(j)}\widetilde{\psi}^{(A)}_{a\alpha}, \qquad \overline{q}^A_{a\alpha j} = \overline{\widetilde{\psi}}^{(A)}_{a\alpha}\,\gamma_4\,D^{(j)\dagger}, \tag{19}$$

where a is a color index, α is a Dirac spin component, j is a displacement type, and A is a quark flavor. To simplify notation, the Dirac spin component and the displacement type are combined into a single index in what follows.

Each baryon operator destroying a three-momentum $\boldsymbol{p}$ is a linear superposition of so-called elemental three-quark operators, which are gauge-invariant terms of the form

$$\Phi^{ABC}_{\alpha\beta\gamma}(\boldsymbol{p},t) = \sum_{\boldsymbol{x}} e^{-i\boldsymbol{p}\cdot\boldsymbol{x}}\varepsilon_{abc}\,q^A_{a\alpha}(\boldsymbol{x},t)\,q^B_{b\beta}(\boldsymbol{x},t)\,q^C_{c\gamma}(\boldsymbol{x},t).$$

The "barred" three-quark elemental operators which create a momentum $\boldsymbol{p}$ have the form

$$\overline{\Phi}^{ABC}_{\alpha\beta\gamma}(\boldsymbol{p},t) = \sum_{\boldsymbol{x}} e^{i\boldsymbol{p}\cdot\boldsymbol{x}}\varepsilon_{abc}\,\overline{q}^C_{c\gamma}(\boldsymbol{x},t)\,\overline{q}^B_{b\beta}(\boldsymbol{x},t)\,\overline{q}^A_{a\alpha}(\boldsymbol{x},t).$$

We use hadron operators which transform irreducibly under all symmetries of the three-dimensional cubic lattice. Each baryon sink operator, being a linear superposition of the three-quark elemental operators, has the form

$$B_l(t) = c^{(l)}_{\alpha\beta\gamma}\;\Phi^{ABC}_{\alpha\beta\gamma}(t), \tag{20}$$

where l is a compound index comprised of a three-momentum $\boldsymbol{p}$, an irreducible representation (irrep) Λ of the lattice symmetry group, the row λ of the irrep, isospin and other flavor quantum numbers, and an identifier labeling the different operators in each symmetry channel. The corresponding source operators are

$$\overline{B}_l(t) = c^{(l)*}_{\alpha\beta\gamma}\;\overline{\Phi}^{ABC}_{\alpha\beta\gamma}(t). \tag{21}$$

The baryon correlation matrix elements are given by

$$C_{l\bar{l}}(t_F - t_0) = \frac{1}{N_t}\sum_{t_0}\langle\; B_l(t_F)\;\overline{B}_{\bar{l}}(t_0)\;\rangle, \tag{22}$$

where $\langle\ldots\rangle$ denotes a vacuum expectation value, which is given by the usual ratio of path integrals over the fermion and gauge fields Wick-rotated into imaginary time. To simplify notation, we replace the average over all source times by a single fixed time t_0, exploiting time-translation invariance, and obtain

$$C_{l\bar{l}}(t_F - t_0) = c^{(l)}_{\alpha\beta\gamma}c^{(\bar{l})*}_{\overline{\alpha\beta\gamma}}\langle\;\Phi^{ABC}_{\alpha\beta\gamma}(t_F)\;\overline{\Phi}^{\overline{ABC}}_{\overline{\alpha\beta\gamma}}(t_0)\;\rangle.$$

Expand the three-quark elemental operators in terms of the covariantly-displaced smeared quark fields,

$$\begin{aligned} C_{l\bar{l}}(t_F - t_0) &= c^{(l)}_{\alpha\beta\gamma}c^{(\bar{l})*}_{\overline{\alpha\beta\gamma}}\sum_{\boldsymbol{x}\overline{\boldsymbol{x}}}\;\varepsilon_{abc}\;\varepsilon_{\overline{abc}}e^{-i\boldsymbol{p}\cdot(\boldsymbol{x}-\overline{\boldsymbol{x}})} \\ &\times\langle\, q^A_{a\alpha}(\boldsymbol{x},t_F)\,q^B_{b\beta}(\boldsymbol{x},t_F)\,q^C_{c\gamma}(\boldsymbol{x},t_F) \\ &\quad\times\overline{q}^{\overline{C}}_{\overline{c\gamma}}(\overline{\boldsymbol{x}},t_0)\;\overline{q}^{\overline{B}}_{\overline{b\beta}}(\overline{\boldsymbol{x}},t_0)\;\overline{q}^{\overline{A}}_{\overline{a\alpha}}(\overline{\boldsymbol{x}},t_0)\;\rangle, \end{aligned}$$

where the three-momenta associated with l and $\bar{l}$ are assumed to be the same $\boldsymbol{p}$, then evaluate the path integrals over the Grassmann fields to obtain a sum over products of quark lines, defining $t = t_F - t_0$:

$$\begin{aligned} C_{l\bar{l}}(t) &= c^{(l)}_{\alpha\beta\gamma}c^{(\bar{l})*}_{\overline{\alpha\beta\gamma}}\sum_{\boldsymbol{x}\overline{\boldsymbol{x}}}\;\varepsilon_{abc}\;\varepsilon_{\overline{abc}}e^{-i\boldsymbol{p}\cdot(\boldsymbol{x}-\overline{\boldsymbol{x}})} \\ &\times\;\Big\langle\mathcal{Q}^{(A\overline{A})}_{a\alpha;\overline{a\alpha}}\mathcal{Q}^{(B\overline{B})}_{b\beta;\overline{b\beta}}\mathcal{Q}^{(C\overline{C})}_{c\gamma;\overline{c\gamma}} - \mathcal{Q}^{(A\overline{A})}_{a\alpha;\overline{a\alpha}}\mathcal{Q}^{(B\overline{C})}_{b\beta;\overline{c\gamma}}\mathcal{Q}^{(C\overline{B})}_{c\gamma;\overline{b\beta}} \\ &-\;\mathcal{Q}^{(A\overline{B})}_{a\alpha;\overline{b\beta}}\mathcal{Q}^{(B\overline{A})}_{b\beta;\overline{a\alpha}}\mathcal{Q}^{(C\overline{C})}_{c\gamma;\overline{c\gamma}} - \mathcal{Q}^{(A\overline{C})}_{a\alpha;\overline{c\gamma}}\mathcal{Q}^{(B\overline{B})}_{b\beta;\overline{b\beta}}\mathcal{Q}^{(C\overline{A})}_{c\gamma;\overline{a\alpha}} \\ &+\;\mathcal{Q}^{(A\overline{C})}_{a\alpha;\overline{c\gamma}}\mathcal{Q}^{(B\overline{A})}_{b\beta;\overline{a\alpha}}\mathcal{Q}^{(C\overline{B})}_{c\gamma;\overline{b\beta}} + \mathcal{Q}^{(A\overline{B})}_{a\alpha;\overline{b\beta}}\mathcal{Q}^{(B\overline{C})}_{b\beta;\overline{c\gamma}}\mathcal{Q}^{(C\overline{A})}_{c\gamma;\overline{a\alpha}}\Big\rangle_U, \end{aligned}$$

where time and spatial labels have been omitted, and $\langle\ldots\rangle_U$ is an expectation value defined as a ratio of path integrals over the gauge field U only, using the gauge field action and the fermion determinant as the path integral weight. Note that each quark propagator $\mathcal{Q}$ connects each source site $\overline{\boldsymbol{x}}$ to each sink site $\boldsymbol{x}$, as well as connecting color and spin components between the source and sink. Hence, the summations in the above equation are quite costly to carry out, and must be repeated over and over again for every pair of baryon operators.

A dramatic simplification of the above equation can be achieved by using Eq. (15) to estimate each quark line. The following quantity emerges as a key component of the resulting estimate:

$$\begin{aligned} \mathcal{B}^{[b_1b_2b_3]}_l(\varphi_1,\varphi_2,\varphi_3;t) &= c^{(l)}_{\alpha\beta\gamma}\sum_{\boldsymbol{x}}\;e^{-i\boldsymbol{p}\cdot\boldsymbol{x}}\varepsilon_{abc} \\ &\times\varphi^{[b_1]}_{a\alpha\boldsymbol{x}t}(\rho_1)\;\varphi^{[b_2]}_{b\beta\boldsymbol{x}t}(\rho_2)\;\varphi^{[b_3]}_{c\gamma\boldsymbol{x}t}(\rho_3), \end{aligned} \tag{23}$$

where b_1, b_2, b_3 are noise dilution projector indices, and the short-hand notation $\varphi_k = \varphi(\rho_k)$ has been used, where φ is the quantity defined in Eq. (14). The baryon correlation matrix element is then given by

$$\begin{aligned} C_{l\bar{l}}(t_F - t_0) \;=\; &\Big\langle\mathcal{B}^{[b_1b_2b_3]}_l(\varphi_1,\varphi_2,\varphi_3;t_F) \\ &\times\;\Big(\delta^{\overline{ABC}}_{ABC}\;\mathcal{B}^{[b_1b_2b_3]}_{\bar{l}}(\varrho_1,\varrho_2,\varrho_3;t_0) \\ &-\;\delta^{\overline{ACB}}_{ABC}\;\mathcal{B}^{[b_1b_3b_2]}_{\bar{l}}(\varrho_1,\varrho_3,\varrho_2;t_0) \\ &-\;\delta^{\overline{BAC}}_{ABC}\;\mathcal{B}^{[b_2b_1b_3]}_{\bar{l}}(\varrho_2,\varrho_1,\varrho_3;t_0) \\ &-\;\delta^{\overline{CBA}}_{ABC}\;\mathcal{B}^{[b_3b_2b_1]}_{\bar{l}}(\varrho_3,\varrho_2,\varrho_1;t_0) \\ &+\;\delta^{\overline{CAB}}_{ABC}\;\mathcal{B}^{[b_2b_3b_1]}_{\bar{l}}(\varrho_2,\varrho_3,\varrho_1;t_0) \\ &+\;\delta^{\overline{BCA}}_{ABC}\;\mathcal{B}^{[b_3b_1b_2]}_{\bar{l}}(\varrho_3,\varrho_1,\varrho_2;t_0)\Big)^*\Big\rangle_{U,\rho} \end{aligned} \tag{24}$$

where $\delta^{DEF}_{ABC} = \delta_{AD}\delta_{BE}\delta_{CF}$ and $\langle\ldots\rangle_{U,\rho}$ indicates an expectation value over the gauge field U and any Z_N noises ρ_k. Again, the above equation uses the short-hand notation $\varphi_k = \varphi(\rho_k)$ and $\varrho_k = \varrho(\rho_k)$, where the quark sinks φ are defined in Eq. (14) and the quark sources ϱ are defined in Eq. (13). A, B, C are the quark flavors of the first, second, and third quarks as ordered in the $\mathcal{B}$ functions. To increase statistics, an average of the six permutations of the $1, 2, 3$ superscripts labeling the quark lines

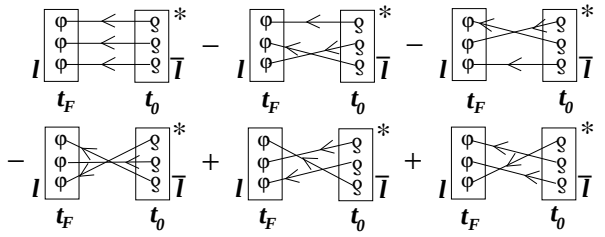

FIG. 7: Graphical depiction of Eq. (24) for a baryon correlator $C_{l\overline{l}}(t_F - t_0)$ with source time t_0 and later sink time t_F. Each box represents a baryon function given by Eq. (23) with the first quark located at the top of the box. Lines connecting a ϱ with a φ indicate summation over their dilution projector identifiers. The same noise must be used at the two ends of any single line, and different noises should be used for different lines. Any line connecting quarks of different flavors represents a zero value. The asterisks indicate complex conjugation.

can be used, and if the masses of all three quark lines are the same, this requires no further inversions of the Dirac matrix.

A very useful feature of Eq. (24) is the fact that the baryon correlator completely factorizes into a function associated with the sink time slice t_F, and another function associated with the source time slice t_0. Summations over color, spin, and spatial sites at the source have been completely separated from the color, spin, and spatial summations at the sink. The stochastic LapH method leads to complete factorization of hadron sources and sinks in temporal correlations, which greatly simplifies the logistics of evaluating correlation matrices involving large numbers of operators. Eq. (24) also shows that implementing the Wick contractions of the quark lines is also straightforward. Contributions from different Wick orderings within a class of quark-line diagrams differ only by permutations of the noises at either the source or the sink. In Eq. (24), permutations of the noises at the source have been used since this is generally much less costly.

Given the plethora of indices, a graphical representation of the above equation is useful and is shown in Fig. 7. The quark field ψ is represented by a quark sink φ or a $\overline{\varrho}$, and $\overline{\psi}$ becomes a ϱ or a $\overline{\varphi}$. We represent a baryon given by Eq. (23) by a box containing the quark sources or sinks vertically aligned with the first quark on the left in Eq. (23) located at the top of the box. We use lines connecting a ϱ with a φ (or a $\overline{\varrho}$ with a $\overline{\varphi}$) to denote summation over the dilution indices associated with the connected ϱ and φ. The same noise must be used at the two ends of any single line, and different noises should be used for different lines.

B. Meson to meson correlations

Each meson operator destroying a three-momentum $\boldsymbol{p}$ is a linear superposition of quark-antiquark elemental operators which are linear superpositions of gauge-invariant

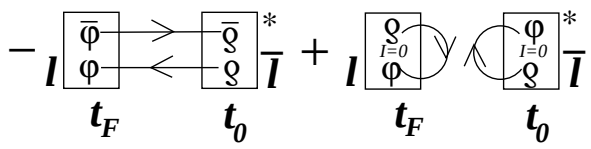

FIG. 8: Graphical depiction of Eq. (33) for a meson correlator $C_{l\overline{l}}(t_F - t_0)$ with source time t_0 and later sink time t_F. Each box represents a meson function given by Eq. (32) with the first quark field located at the top of the box. Lines connecting a ϱ with a φ or a $\overline{\varrho}$ with a $\overline{\varphi}$ indicate summation over their dilution projector identifiers. The same noise must be used at the two ends of any single line, and different noises should be used for different lines. Any line connecting quarks of different flavors represents a zero value. The asterisks indicate complex conjugation. Contributions from the meson internal lines occur only for isoscalar mesons.

terms of the form

$$\Phi^{AB}_{\alpha\beta}(t) = \sum_{\boldsymbol{x}} e^{-i\boldsymbol{p}\cdot(\boldsymbol{x}+\frac{1}{2}(\boldsymbol{d}_\alpha+\boldsymbol{d}_\beta))}\delta_{ab}\ \overline{q}^A_{a\alpha}(\boldsymbol{x},t)\ q^B_{b\beta}(\boldsymbol{x},t), \tag{25}$$

where $q, \overline{q}$ are defined in Eq. (19), $\boldsymbol{d}_\alpha, \boldsymbol{d}_\beta$ are the spatial displacements of the $\overline{q}, q$ fields, respectively, from $\boldsymbol{x}$, A, B indicate flavor, and α, β are compound indices incorporating both spin and quark-displacement types. The phase factor involving the quark-antiquark displacements is needed to ensure proper transformation properties under G-parity for arbitrary displacement types. The "barred" operators which create a momentum $\boldsymbol{p}$ then take the form

$$\overline{\Phi}^{AB}_{\alpha\beta}(t) = \sum_{\boldsymbol{x}} e^{i\boldsymbol{p}\cdot(\boldsymbol{x}+\frac{1}{2}(\boldsymbol{d}_\alpha+\boldsymbol{d}_\beta))}\delta_{ab}\ \overline{q}^B_{b\beta}(\boldsymbol{x},t)\ q^A_{a\alpha}(\boldsymbol{x},t). \tag{26}$$

Each meson sink operator has the form

$$M_l(t) = c^{(l)}_{\alpha\beta}\ \Phi^{AB}_{\alpha\beta}(t), \tag{27}$$

(or is a flavor combination of the above form), where again, the l label includes the momentum $\boldsymbol{p}$, the symmetry group irrep Λ, the row λ of the irrep, and an identifier specifying the different operators in each symmetry channel. The corresponding source operators are

$$\overline{M}_l(t) = c^{(l)*}_{\alpha\beta}\ \overline{\Phi}^{AB}_{\alpha\beta}(t). \tag{28}$$

The meson correlation matrix elements are given by

$$C_{l\overline{l}}(t_F - t_0) = \frac{1}{N_t}\sum_{t_0} \langle\ M_l(t_F)\ \overline{M_{\overline{l}}}(t_0)\ \rangle. \tag{29}$$

In terms of the elemental operators and using translation invariance, the above equation becomes,

$$C_{l\overline{l}}(t_F - t_0) = c^{(l)}_{\alpha\beta} c^{(\overline{l})*}_{\overline{\alpha}\overline{\beta}} \langle\ \Phi^{AB}_{\alpha\beta}(t_F)\ \overline{\Phi}^{\overline{AB}}_{\overline{\alpha}\overline{\beta}}(t_0)\ \rangle, \tag{30}$$

using translation invariance to fix to a single t_0 for notational convenience. Expand the elemental operators in

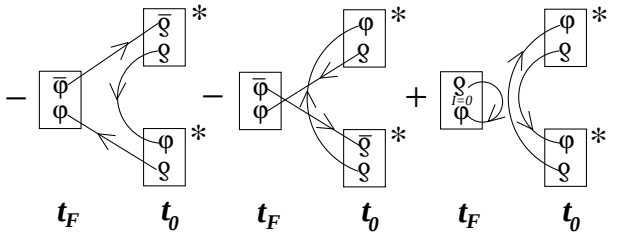

FIG. 9: Computation of the temporal correlation of a two-meson source at time t_0 and a single-meson sink at time t_F. The source mesons are assumed to be non-isoscalars. Each box represents a meson function given by Eq. (32) with the first quark field located at the top of the box. Lines connecting a ϱ with a φ or a $\overline{\varrho}$ with a $\overline{\varphi}$ indicate summation over their dilution projector identifiers. The same noise must be used at the two ends of any single line, and different noises should be used for different lines. Any line connecting quarks of different flavors represents a zero value. The asterisks indicate complex conjugation. The diagram with an internal line contributes only for isoscalar mesons.

terms of the covariantly-displaced smeared quark fields:

$$C_{l\overline{l}}(t_F-t_0) = c^{(l)}_{\alpha\beta} c^{(\overline{l})*}_{\overline{\alpha}\overline{\beta}} \sum_{\boldsymbol{x}\overline{\boldsymbol{x}}} e^{-i\boldsymbol{p}\cdot(\boldsymbol{x}+\frac{1}{2}(\boldsymbol{d}_\alpha+\boldsymbol{d}_\beta))} \times e^{i\boldsymbol{p}\cdot(\overline{\boldsymbol{x}}+\frac{1}{2}(\boldsymbol{d}_{\overline{\alpha}}+\boldsymbol{d}_{\overline{\beta}}))} \langle\ \overline{q}^A_{a\alpha}(\boldsymbol{x},t_F)\ q^B_{a\beta}(\boldsymbol{x},t_F) \times \overline{q}^{\overline{B}}_{\overline{a}\overline{\beta}}(\overline{\boldsymbol{x}},t_0)\ q^{\overline{A}}_{\overline{a}\overline{\alpha}}(\overline{\boldsymbol{x}},t_0)\ \rangle,$$

where the three-momenta associated with l and $\overline{l}$ are assumed to be the same $\boldsymbol{p}$. Next, the path integrals over the Grassmann fields are carried out, and one obtains, for $t = t_F - t_0$,

$$C_{l\overline{l}}(t) = c^{(l)}_{\alpha\beta} c^{(\overline{l})*}_{\overline{\alpha}\overline{\beta}} \sum_{\boldsymbol{x}\overline{\boldsymbol{x}}} e^{-i\boldsymbol{p}\cdot(\boldsymbol{x}+\frac{1}{2}(\boldsymbol{d}_\alpha+\boldsymbol{d}_\beta))} \times e^{i\boldsymbol{p}\cdot(\overline{\boldsymbol{x}}+\frac{1}{2}(\boldsymbol{d}_{\overline{\alpha}}+\boldsymbol{d}_{\overline{\beta}}))} \Big\langle -\mathcal{Q}^{(\overline{A}A)}_{\overline{a\alpha};a\alpha}\ \mathcal{Q}^{(B\overline{B})}_{a\beta;\overline{a}\overline{\beta}} + \mathcal{Q}^{(BA)}_{a\beta;a\alpha}\ \mathcal{Q}^{(\overline{AB})}_{\overline{a\alpha};\overline{a}\overline{\beta}} \Big\rangle_U, \quad (31)$$

omitting time and spatial labels. Eq. (15) or Eq. (16) can then be used to estimate the two quark propagators. In the first term, we find that it is advantageous to use Eq. (16) for the A quark line and Eq. (15) for the B quark line.

To proceed, define the following meson function:

$$\mathcal{M}^{[b_1b_2]}_l(\varrho_1,\varphi_2;t) = c^{(l)}_{\alpha\beta} \sum_{\boldsymbol{x}}\ e^{-i\boldsymbol{p}\cdot(\boldsymbol{x}+\frac{1}{2}(\boldsymbol{d}_\alpha+\boldsymbol{d}_\beta))} \times \varrho^{[b_1]}_{a\alpha\boldsymbol{x}t}(\rho_1)^*\ \varphi^{[b_2]}_{a\beta\boldsymbol{x}t}(\rho_2), \quad (32)$$

where b_1, b_2 are noise dilution projector indices, and the short-hand notation $\varphi_k = \varphi(\rho_k)$ has been used again. The meson correlator is given by

$$C_{l\overline{l}}(t_F-t_0) = \Big\langle -\delta^{\overline{AB}}_{AB}\ \mathcal{M}^{[b_1b_2]}_l(\overline{\varphi}_1,\varphi_2;t_F)\ \mathcal{M}^{[b_1b_2]}_{\overline{l}}(\overline{\varrho}_1,\varrho_2;t_0)^* + \delta^{B\overline{B}}_{A\overline{A}}\ \mathcal{M}^{[b_1b_1]}_l(\varrho_1,\varphi_1;t_F)\ \mathcal{M}^{[b_2b_2]}_{\overline{l}}(\varphi_2,\varrho_2;t_0)^* \Big\rangle_{U,\rho} \quad (33)$$

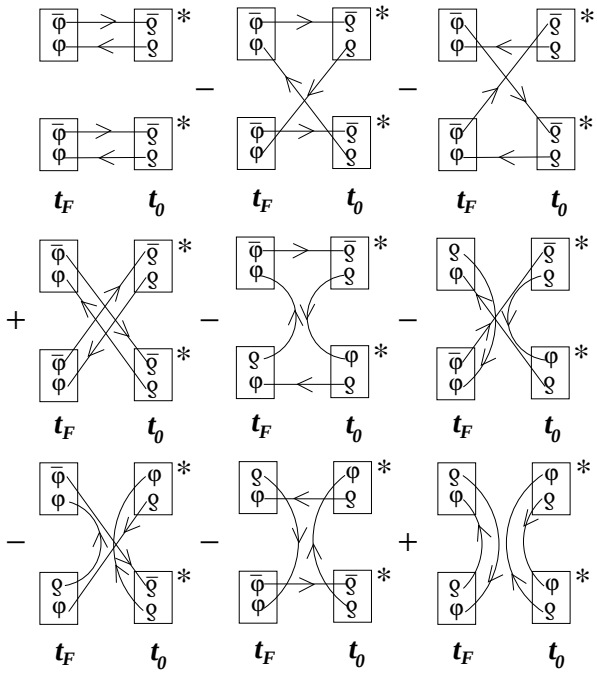

FIG. 10: Computation of the temporal correlation of a two-meson source at time t_0 with a two-meson sink at time t_F. All four mesons are assumed to be non-isoscalars. Each box represents a meson function given by Eq. (32) with the first quark field located at the top of the box. Lines connecting a ϱ with a φ or a $\overline{\varrho}$ with a $\overline{\varphi}$ indicate summation over their dilution projector identifiers. The same noise must be used at the two ends of any single line, and different noises should be used for different lines. Any line connecting quarks of different flavors represents a zero value. The asterisks indicate complex conjugation.

where $\delta^{CD}_{AB} = \delta_{AC}\delta_{BD}$. The second term only contributes to isoscalar mesons. Again, color, spin, and spatial summations at the sink have completely factorized from the summations at the source. This equation is graphically represented in Fig. 8.

C. More complicated correlations

The graphical rules developed in the preceding sections can be applied to more complicated correlation matrix elements. The correlation of a two meson source with a single-meson sink is represented in Fig. 9. The source mesons are assumed to be non-isoscalars, otherwise there would be additional diagrams involving meson internal lines. The correlation of a two-meson source with a two-meson sink is illustrated in Fig. 10. All four mesons are assumed to be non-isoscalars. We apply γ_5 Hermiticity only in cases where a $\psi(t_0)$ at the source connects with a $\overline{\psi}(t_F)$ at the sink. Full time dilution is the best choice for all quark lines connecting t_0 and t_F and t_0 to t_0. For

all t_F-to-t_F quark lines, interlacing in source time must be used.

To evaluate any correlation matrix element using the stochastic LapH method, one first must identify the various hadron functions that are needed and calculate them using Eqs. (23) and (32). These can be evaluated for a large set of hadron operators and stored on disk. The quark propagators are needed only at this stage of the computation. All color contractions and spatial sums are carried out in evaluating the hadron functions. Each hadron function for a given choice of noises takes up very little space on disk since each is an array over time and dilution indices only. The correlation matrix elements are then combinations of the different hadron functions for different noise selections. These final contractions involve only summations of dilutions indices. In this way, a large number of correlation matrices can be evaluated very efficiently.

IV. IMPLEMENTATION DETAILS

Our software is written in C++ and links to the USQCD QDP++/Chroma library[27]. Parts of our computations must be done using the full four-dimensional lattice, but other parts are best handled time slice by time slice in three dimensions. QDP++ does not handle both three and four dimensional lattices simultaneously, so the different parts of the computations were done in separate runs using both 3d and 4d versions of our software. Special input/output routines were written to enable 4d QDP++ to read and write 3d time slices of the lattice.

Our computations are done as a sequence of tasks for each gauge configuration in the Monte Carlo ensemble. In the first task, the spatial links of the gauge configuration are smeared using the stout-link procedure. This task is done using a four-dimensional version of our software, but the smeared spatial links are written to disk as individual time slices suitable for input to the three-dimensional version of our software. In the second task, computation of the Laplacian eigenvectors is done time slice by time slice in three dimensions. In the third task, the eigenvectors for the different time slices are reorganized into four-dimensional eigenvectors corresponding to the different eigenvalues. The fourth task is the computation of the quark propagators. The inversions of the Dirac matrix must be done using the full four-dimensional lattice, but our results are written to disk once again as three-dimensional time slices. Formation of the hadron sources and sinks is accomplished in the fifth task using the three-dimensional version of our software. All of our hadron operators have definite three momenta which involve summations over all spatial sites of the lattice, so the resulting hadron sources and sinks are no longer lattice quantities. The final task is the assembly of the hadron sinks and sources to form the hadron correlation functions which can be accomplished using a serial version of our software.

The eigenvectors of the gauge-covariant Laplacian are evaluated using a Krylov-Spectral Restarted Lanczos (KSRL) method which is a modification of the thick restarted Lanczos method described in Ref. [28]. Let A denote a Hermitian matrix whose lowest-lying or highest-lying eigenvectors are sought. Given a starting vector u, the KSRL method begins by constructing a Krylov space spanned by vectors $u, Au, A^2u, \ldots, A^mu$. The submatrix of A defined in this basis is then diagonalized, and the eigenvalues and eigenvectors of this submatrix, known as the Ritz values and Ritz vectors, are approximations to those of the full matrix A. Convergence to the exact eigenpairs occurs as the Krylov space dimension increases, but a better procedure is to stop the growth of the Krylov space at some point, typically just above the number of desired eigenpairs, and restart the procedure using a different starting vector or vectors. The use of a certain number of Ritz vectors to restart the procedure is known as Krylov-Spectral restarting. Key issues in the method are determining how many Ritz vectors to use in restarting, determining the size of the Krylov space to use, and maintaining orthogonality of the Lanczos vectors in finite-precision mathematics.

In our calculations, we use either a random vector or the vector whose components are all equal for the starting vector. Full global reorthogonalization is used at all steps. The decision to reorthogonalize multiple times is based on a simple criterion[29]: if the norm of the vector decreases by $1/\kappa$, where $\kappa = \sqrt{2}$, then further reorthgonalization is done. A maximum of four reorthogonalizations is enforced. Equation 5 in Ref. [30] is used to choose the number of Ritz vectors to keep, except that the number must be at least as large as the number of converged vectors and cannot exceed the dimension of the Krylov space minus the number of converged and locked vectors minus twelve. For an approximate eigenvector x (with unit norm) and an estimate λ of its corresponding eigenvalue, the residual norm is defined by $r = ||Ax - \lambda x||$. An eigenpair is considered converged when $r < \texttt{tol}||A||$, where `tol` is the desired tolerance and the matrix 2-norm is defined by $||A|| = \max_{x\neq 0} ||Ax||/||x||$, and can be estimated by the largest absolute value of any Ritz value encountered in the computation.

In calculating the eigenvectors of $\widetilde{\Delta}$, Chebyshev acceleration is used. The eigenvalues of $-\widetilde{\Delta}$ are all real and lie between 0 and some maximum value denoted by λ_L. We wish to determine the eigenvectors corresponding to the lowest-lying eigenvalues lying between 0 and some cutoff λ_C. The rate of convergence to solution increases with the spacing between the levels. Convergence is much faster for widely spaced levels. Hence, convergence can be accelerated by transforming the spectrum so that the desired part of the spectrum is more widely spaced. The following transformation is applied first:

$$B = 1 + \frac{2}{(\lambda_L - \lambda_C)}\Big(\widetilde{\Delta} + \lambda_C\Big). \tag{34}$$

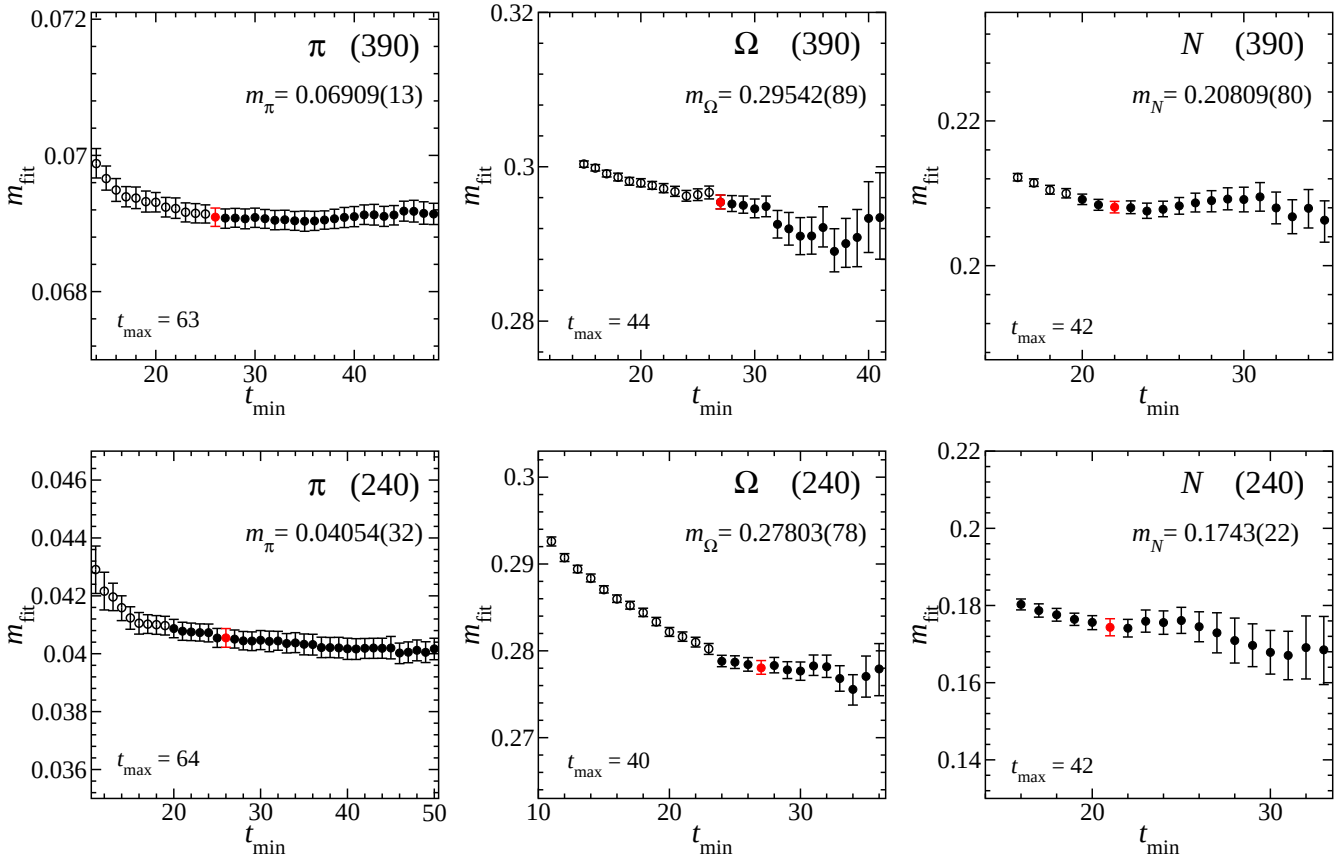

FIG. 11: Masses $m_{\rm fit}(t)$ obtained by fitting the correlators for single-site π, Ω, N operators to a cosh(exponential) form for the $\pi(\Omega, N)$ in the temporal range $t_{\rm min}$ to $t_{\rm max}$. Results are shown for different $t_{\rm min}$ with $t_{\rm max}$ fixed to the value stated in the lower left corner of each plot. Open symbols indicate unacceptable fit qualities, and solid symbols show results with acceptable fit qualities Q. The top row shows results using 551 configurations of the 390 ensemble on a $24^3 \times 128$ lattice, and the bottom row shows results with 584 configurations of the 240 ensemble on a $24^3 \times 128$ lattice. The fit value given in each plot corresponds to the fit indicated by the red point.

The above transformation maps the unwanted spectrum to the range $-1 \cdots 1$, and the desired part lies above 1. Chebyshev polynomials are then applied:

$$A = T_n(B). \tag{35}$$

Eigenvalues lying between -1 and 1 stay between -1..1, and the desired eigenvalues above 1 get spaced out to large and widely-separated values above 1. The lowest-lying eigenvalue of $-\widetilde{\Delta}$ becomes the highest-lying eigenvalue of A. Transforming the desired levels to the region above 1 is most convenient since it allows the use of Chebyshev polynomials of any order, both even and odd. The Chebyshev polynomials are applied using the following recurrence relation:

$$T_0(x) = 1, \qquad T_1(x) = x, \tag{36}$$
$$T_n(x) = 2x\, T_{n-1}(x) - T_{n-2}(x). \tag{37}$$

For calculations done on our anisotropic $24^3 \times 128$ lattices, we need to compute the lowest-lying $N_v = 112$ eigenvectors on each time slice. A Krylov space dimension of 160 was found to work well, and $\lambda_L = 15$ and $\lambda_C = 0.5$ were appropriate. Chebyshev polynomials of order 8 were used, and the residual tolerance was set to 10^{-9}. Convergence of all N_v levels occurred within a dozen or less restarts.

The LapH eigenvectors are uniquely determined only to within an overall phase. Given the way in which Z_N noise is injected in the LapH subspace, one sees that a given quark line is not invariant under a change of the phase multiplying each eigenvector (due to the off-diagonal pieces not being exactly zero). It turns out that changing the phase is equivalent to changing the noise by a U(1) phase. This is not a problem, but erroneous results can occur if the original eigenvector files used to determine the quark sinks get deleted and the eigenvectors have to be reconstructed for making the hadrons. With different run parameters, the eigensolver could produce a different phase. The introduction of a phase convention eliminates this potential problem.

Once the needed eigenvectors of the Laplacian are computed and stored, the next step is to compute all elements of $V_s^\dagger \Omega^{-1} V_s P^{[b]} \rho^r$. There are only $N_t N_v$ elements

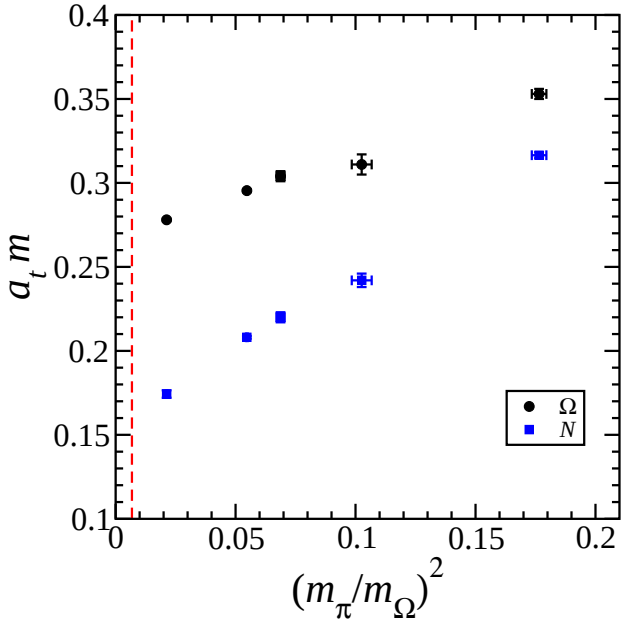

FIG. 12: Products of a_t and the nucleon and Ω-baryon masses against $(m_\pi/m_\Omega)^2$ for fixed $\beta = 1.5, m_s = -0.0743$ and varying $m_u = m_d$. The two leftmost points for each baryon are from this work, and the three rightmost points are from Ref. [31]. The vertical dashed line indicates the physical value of $(m_\pi/m_\Omega)^2$.

to store for each noise r and each dilution projector b, so storage of these quark propagation coefficients is modest. Disk storage is actually dominated by the LapH eigenvectors. Another nice feature is the fact that the quark propagation coefficients are gauge invariant, as long as the eigenvector phases are handled appropriately. Solving $\Omega x = y$ for x with $y = V_s P^{[b]} \rho^r$ is accomplished using a mixed-precision improved version of the biconjugate gradient method with even-odd preconditioning. This was found to be the fastest inverter available in Chroma. Occasionally convergence is not achieved, and a slower conjugate gradient solver is applied to the system $\Omega^\dagger \Omega x = \Omega^\dagger y$.

Our correlator estimates and their variances are insensitive to the value of N used for the Z_N noise, as long as N is not too small. We found that $N = 4$ produced results indistinguishable in quality from those of larger N. Hence, we use Z_4 noise in all of our computations. We identify a Z_4 noise vector for an ensemble of gauge configurations by a 16-bit unsigned integer s. To create a noise vector $\rho^{(s)}$ for a gauge configuration labeled by an RHMC trajectory number k (assumed to have a value ranging from 0 to $2^{16} - 1$), a 32-bit unsigned integer m is first formed in a particular manner using the 16 binary digits of s and the 16 bits of k. Although the procedure of forming m is arbitrary, the same procedure must be used in every instance. The 32-bit unsigned integer m is then taken as a seed to the 32-bit Mersenne twister random number generator which is used to create the Z_4 noise $\rho^{(s)}(t, i, \alpha)$ for each LapH eigenvector, labeled by time t and level i, and for each spin index α. The elements of $\rho^{(s)}$ are generated in a particular order that is always the same. Each Z_4 element is chosen using the sequence of bits obtained from the current state of the Mersenne twister, taking two bits at a time. It was found that the linear congruential generator in QDP++/Chroma is not adequate for generating the Z_4 noise and leads to serious errors in some instances.

V. INITIAL APPLICATIONS

Our initial development of the stochastic LapH method was done using a small 16^3 spatial lattice which is not very interesting for hadron physics. Since the main reason for pursuing the method is to apply it on large lattices for both single-hadron and multi-hadron correlators, we proceeded to test the method by studying several simple hadronic systems requiring sink-to-sink quark lines on a reasonably large $24^3 \times 128$ anisotropic lattice having spatial volume $(3\text{ fm})^3$.

Two ensembles of gauge configurations were used. These ensembles were generated using the Rational Hybrid Monte Carlo (RHMC) algorithm[32], which is a variant of the hybrid molecular-dynamics (HMC) algorithm[33] suitable for $N_f = 2 + 1$ quark flavors. The updating algorithm is a Metropolis method with a sophisticated means of proposing a global change to the gauge and pseudofermion fields. A fictitious momentum is introduced for each link variable with a Gaussian distribution and Hamilton's equations involving these momenta and the original action as a potential energy are approximately solved for some length of fictitious time, known as an RHMC trajectory. An improved anisotropic clover fermion action and an improved gauge field action were used[31]. In both ensembles, $\beta = 1.5$ is used and the s quark mass parameter is set to $m_s = -0.0743$ in order to reproduce a specific combination of hadron masses[31]. In one ensemble, the light quark mass parameters are set to $m_u = m_d = -0.0840$ so that the pion mass is around 390 MeV using one particular way of setting the scale, discussed below. In the other ensemble, $m_u = m_d = -0.0860$ are used, resulting in a pion mass around 240 MeV. We refer to these ensembles as the 390 and 240 ensembles, respectively.

We calculated the masses of the pion, the nucleon, and the Ω-baryon. Our results are shown in Fig. 11 for the two ensembles on a $24^3 \times 128$ lattice. This figure demonstrates that the use of our stochastic estimates of the smeared quark propagators still leads to high accuracy results of standard quantities. The nucleon and Ω-baryon masses times a_t are shown in Fig. 12 against $(m_\pi/m_\Omega)^2$. Results from Ref. [31] are also included in this figure. Our goal in this work is simply to present and test the stochastic LapH method, so we defer a detailed analysis of these results until a later publication. However, it is encouraging that fitting the three leftmost Ω-baryon

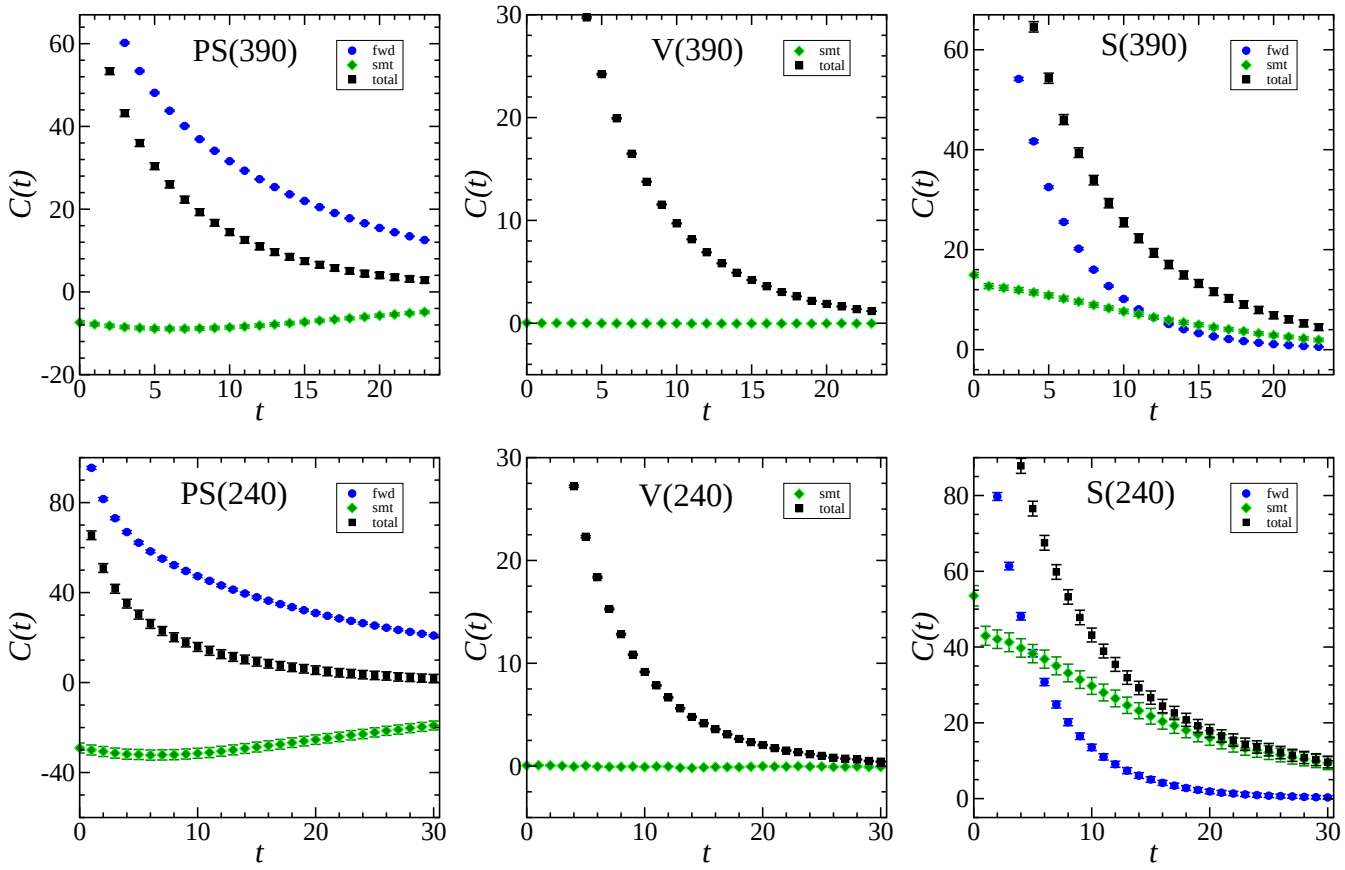

FIG. 13: Correlators $C(t)$ against temporal separation t for single-site operators which produce the isoscalar pseudoscalar (PS), vector (V), and scalar (S) mesons. Results in the top row were obtained using 210 configurations (135 for the scalar channel) of the 390 ensemble. Results in the bottom row were obtained using 198 configurations of the 240 ensemble. In the legends, "fwd" refers to contributions from the diagram containing only forward-time source-to-sink quark lines, "smt" refers to contributions from the diagram containing only quark lines that originate and terminate at the same time. For the scalar channel, the "smt" contribution has a vacuum expectation value subtraction. Forward-time quark lines use dilution scheme (TF, SF, LI8) and same-time quark lines use (TI16, SF, LI8). The lattice size is $24^3 \times 128$ for all the results shown here.

points to a form linear in $(m_\pi/m_\Omega)^2$ and fitting the three leftmost nucleon points to an empirical form linear in m_π/m_Ω yields $m_N/m_\Omega \approx 0.556$ at the physical value of m_π/m_Ω, which compares well with the observed 0.561 value.

Our calculations determine all hadron masses in terms of the temporal lattice spacing a_t. In order to express the hadron masses in terms of MeV, a value of a_t^{-1} must be specified using an appropriate renormalization scheme. Away from the physical point, different renormalization schemes will lead to different choices of a_t^{-1}. One particular scheme that has been used in the past uses the mass of the Ω baryon to set the scale when the strange quark mass is close to the value that reproduces the physical value of $(2m_K^2 - m_\pi^2)/m_\Omega^2$. Using this scheme, we find an inverse temporal spacing $a_t^{-1} = 5.661(17)$ GeV for the 390 ensemble and $a_t^{-1} = 6.015(17)$ GeV for the 240 ensemble. Since the ratio of spatial spacing over temporal spacing has been tuned to a value near 3.5, we have $a_s \sim 0.12$ fm for both of these ensembles. Our values for the pion and nucleon masses are $m_\pi = 0.3911(14)$ GeV and $m_N = 1.1781(58)$ GeV on the 390 ensemble, and $m_\pi = 0.2439(20)$ GeV and $m_N = 1.048(14)$ GeV on the 240 ensemble. An alternative scale-setting scheme would be to extrapolate the Ω-baryon mass results for different m_u, m_d but fixed β, m_s to the physical value of m_π/m_Ω using a form linear in $(m_\pi/m_\Omega)^2$ motivated by heavy baryon chiral perturbation theory, then use the Ω mass to determine a_t^{-1}. Doing this yields $a_t^{-1} \sim 6.3$ GeV and pion masses 250 and 430 MeV for our two ensembles.

Results for the isoscalar mesons in the pseudoscalar, vector, and scalar channels and the two-pion system of total isospin $I = 0, 1, 2$ are presented in Figs. 13, 14, 15, and 16. In these results, the dilution scheme (TF, SF, LI8) is used for all quark lines connecting source time t_0 to the sink time t_F and t_0 to t_0. Four widely-separated source times t_0 were used on each gauge configuration. For all t_F-to-t_F quark lines, the dilution scheme (TI16, SF, LI8) is used. Observables are evaluated using configurations separated by $n_{\rm sep}$ RHMC trajectories, where

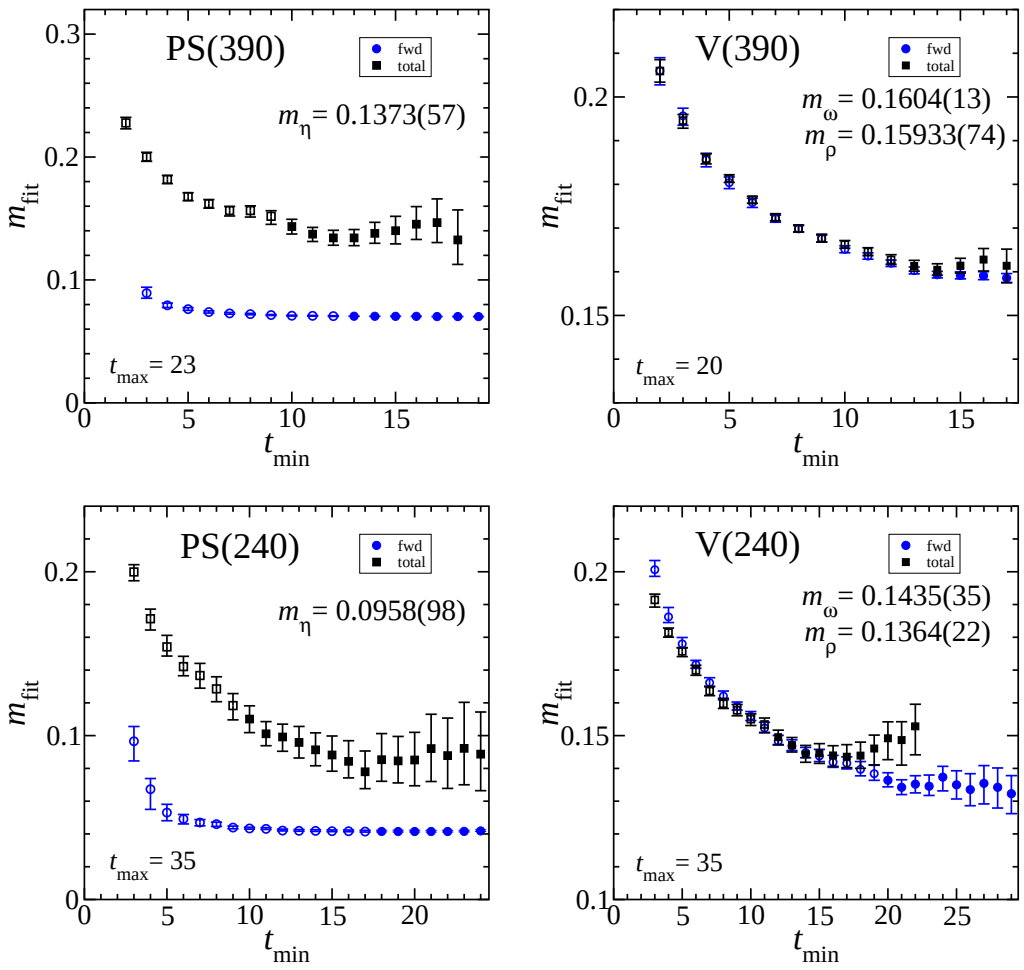

FIG. 14: Masses $m_{\rm fit}(t)$ obtained by fitting the correlators $C(t)$ shown in Fig. 13 to a cosh form in the temporal range $t_{\rm min}$ to $t_{\rm max}$. Results are shown for different $t_{\rm min}$ with $t_{\rm max}$ fixed to the value stated in the lower left corner of each plot. Open symbols indicate unacceptable fit qualities, and solid symbols show results with acceptable fit qualities Q. The top row corresponds to the 390 ensemble, and the bottom row corresponds to the 240 ensemble. The left-hand-side plots show results for the η and π pseudoscalar mesons, and the right-hand-side plots show results for the ω and ρ vector mesons. The scalar channel is not shown here since a reliable extraction of the lowest-lying energy in this channel needs a two-pion operator. The lattice size is $24^3 \times 128$ for all the results shown here.

$n_{\rm sep} = 20$ for the two-pion correlators and $n_{\rm sep} = 40$ for the isoscalar meson correlators. Jackknife binning shows autocorrelations to be suitably small.

Our goal here is simply to test the stochastic LapH method, so simple single-site operators involving only the light u, d quarks are used for the isoscalar mesons, and single-site pion operators are used to make the two-pion states with zero and non-zero relative momenta. The temporal correlations of such simple operators have significant contaminations from higher-lying states, so that the effective masses associated with these correlations tend to a plateau rather slowly. Future work will make use of more sophisticated spatially-extended operators. The issue of mixing with $\overline{s}s$ operators is not addressed in these tests, and no vacuum-expectation-value subtraction is used for the η correlator. In chirally-symmetric fermion formulations, the expectation value of the unsmeared, isosinglet pseudoscalar operator would be proportional to the topological charge, which has notoriously long autocorrelation times and may not be sampled properly in a Monte Carlo simulation[34, 35]. This can show up as a non-zero vacuum expectation value for the η, which disappears as the volume increases. Our test results do not take such effects into account, but future work will investigate this.

In Fig. 13, the contributions to the isoscalar temporal correlations $C(t)$ from the diagram containing only forward-time source-to-sink quark lines are shown with label "fwd", and the contributions from the diagram containing only quark lines that originate and terminate at the same time are shown with label "smt". The total correlator is also shown in each case. In the vector channel, the contribution from the same-time diagram is very small and the total correlator can barely be distinguished

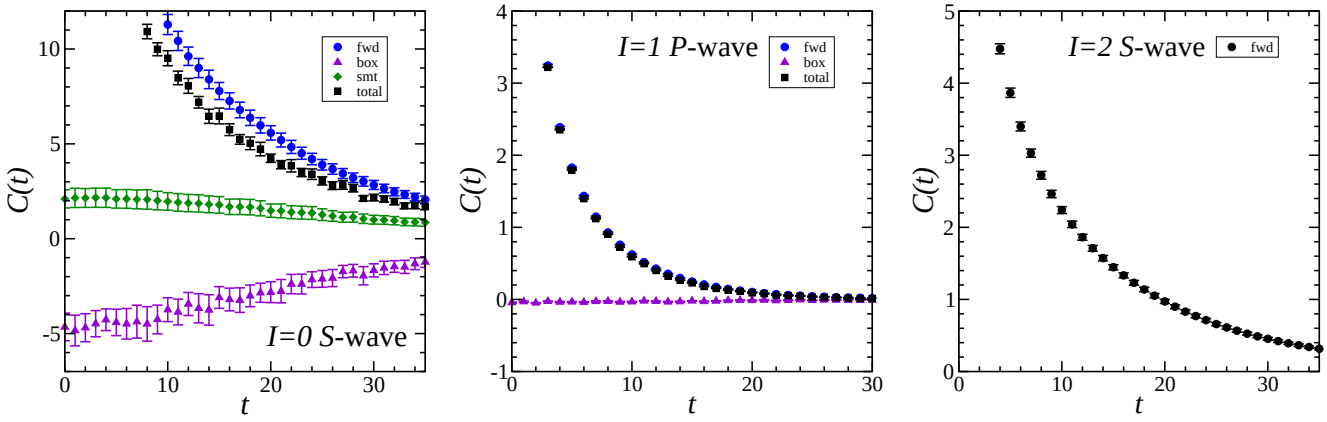

FIG. 15: Correlators $C(t)$ against temporal separation t for two-pion operators with total isospin $I = 0, 1, 2$ and zero total momentum. S-wave results have zero relative momentum, P-wave has minimal non-zero on-axis relative momenta. Results were obtained using 584 configurations of the 240 ensemble. In the legends, "fwd" refers to contributions from diagrams containing only forward-time source-to-sink quark lines, "smt" refers to contributions from diagrams containing only quark lines that originate and terminate at the same time, and "box" refers to diagrams containing both kinds of quark lines. Forward-time quark lines use dilution scheme (TF, SF, LI8) and same-time quark lines use (TI16, SF, LI8). The lattice size is $24^3 \times 128$ for all the results shown here.

from the forward-line diagram contribution, so the "fwd" contribution is not shown. In the scalar channel, the accuracy of the "smt" contribution is particularly remarkable since a large vacuum expectation value has been subtracted.

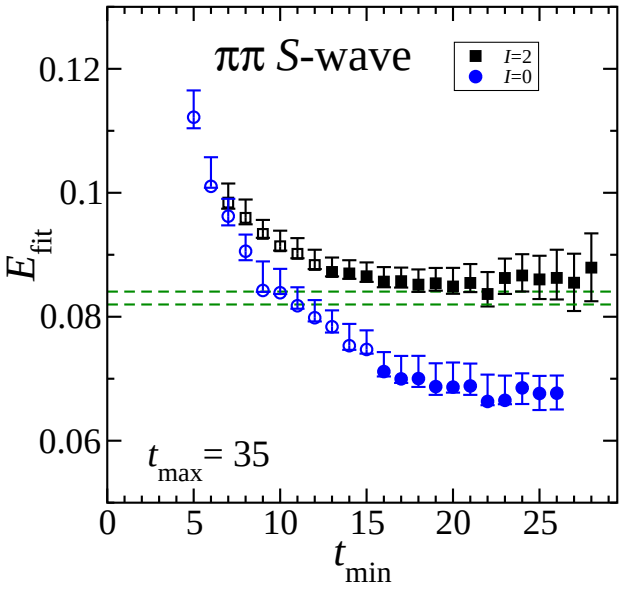

FIG. 16: Energies $E_{\rm fit}(t)$ obtained by fitting the correlators $C(t)$ shown in Fig. 15 to a cosh + constant form in the temporal range $t_{\rm min}$ to $t_{\rm max}$. Results are shown for different $t_{\rm min}$ with $t_{\rm max}$ fixed to the value stated in the lower left corner of the figure. Open symbols indicate unacceptable fit qualities, and solid symbols show results with acceptable fit qualities Q. These results were obtained using 584 configurations of the 240 ensemble. The horizontal dashed lines indicate the energy of two free pions at rest. The lattice size is $24^3 \times 128$.

The correlators in Fig. 13 were used to extract various isoscalar meson masses. The pion and ρ masses can be obtained from the forward-line contributions to the pseudoscalar and vector correlators, respectively. Correlated-χ^2 fits to $A(e^{-mt} + e^{-m(N_t-t)})$ for temporal separations between $t_{\rm min}$ and $t_{\rm max}$ were done to extract the masses of the particles. Jackknife sampling was used to estimate the data covariance matrix, and bootstrap sampling was used to compute the uncertainties in the fit parameters. Results are shown in Fig. 14 for various $t_{\rm min}$ values, with $t_{\rm max}$ fixed to the value stated in each plot. Even using such simple hadron operators, fairly accurate mass extractions are obtained. Future use of better operators will certainly improve these results. Results are not shown for the scalar channel since the lowest-lying energy in this channel is a two-pion state. Extractions of the energies in the scalar channel are best done with a correlator matrix using both single-hadron and two-pion operators. The excellent statistical precision obtained for the correlators at small temporal separations suggests that diagonalizations of future correlation matrices estimated with stochastic LapH will be stable and accurate.

With current Monte Carlo algorithms on presently available computing resources, it remains impractical to use light u, d quark masses tuned to properly reproduce the pion mass. Hence, the u, d quark masses used here yield a pion mass which is too heavy, making comparison to experiment somewhat problematical. Using the Ω-baryon mass to set the inverse temporal spacing, we find masses $m_\eta = 576(59)$ MeV, $m_\rho = 820(13)$ MeV, and $m_\omega = 863(21)$ using 198 configurations of the 240 ensemble. The experimental values are $m_\eta = 548$ MeV, $m_\rho = 776$ MeV, and $m_\omega = 783$ MeV. Future work will use better operators and all 584 configurations to achieve improved results.

Our results for the energies of two light pions are shown in Figs. 15 and 16. We studied S-wave states of zero relative momentum and total isospin $I = 0$ and $I = 2$, as well as a P-wave with minimal non-zero on-axis relative momenta in the $I = 1$ channel. In Fig. 15, contributions to the correlators from the diagrams containing only forward-time source-to-sink quark lines are labeled by "fwd", contributions from diagrams containing only quark lines that originate and terminate at the same time are shown as "smt", and contributions labeled by "box" are those from the diagrams containing both kinds of quark lines (see Fig. 10). Energies were extracted using correlated-χ^2 fits to the form $A + B(e^{-Et} + e^{-E(N_t-t)})$ in the range $t_{\rm min}$ to $t_{\rm max}$. The results for different $t_{\rm min}$ are shown in Fig. 16, for $t_{\rm max}$ fixed to the value stated in the figure. Open symbols indicate unacceptable fit qualities, whereas solid symbols indicate results from fits of acceptable quality Q. The constant term in the fit form arises from a source pion propagating forward in time interacting with a sink pion propagating backwards in time and other similar contributions. The constant term was clearly evident in the $I = 2$ channel, but was consistent with zero in the $I = 0$ channel. Hence, the $I = 0$ results shown in Fig. 15 were done setting the constant term to zero. This figure demonstrates that the stochastic LapH method can provide sufficient accuracy to see the difference of these two-pion energies from the energy of two free pions at rest, indicated by the horizontal dashed lines. In the $I = 1$ channel, the ρ-meson is expected to be the lowest-lying energy level, so a correlator matrix including single-hadron and two-pion operators is necessary to reliably extract the low-lying spectrum in this channel. This will be done in future work. Again, we emphasize that only very simple operators were used here, and future use of better operators will improve the accuracy of these energies.

VI. CONCLUSION

A new method of stochastically estimating the low-lying effects of quark propagation was proposed which allows accurate determinations of temporal correlations of single-hadron and multi-hadron operators in lattice QCD. The method enables accurate treatment of hadron correlators involving quark propagation from all spatial sites on one time slice to all spatial sites on another time slice. Contributions involving quark lines originating at the sink time t_F and terminating at the same sink time t_F are easily handled, even for a large number of t_F times.

The effectiveness of the method can be traced to two of its key features: the use of noise dilution projectors that interlace in time and the use of Z_N noise in the subspace defined by the Laplacian Heaviside quark-field smearing. Introducing noise in the LapH subspace results in greatly reduced variances in temporal correlations compared to methods that introduce noise on the entire lattice. Although the number of Laplacian eigenvectors needed to span the LapH subspace rises dramatically with the spatial volume, we found that the number of inversions of the Dirac matrix needed for a target accuracy was remarkably insensitive to the lattice volume, once a sufficient number of dilution projectors were introduced.

In addition to increased efficiency, the stochastic LapH method has other advantages. The method leads to complete factorization of hadron sources and sinks in temporal correlations, which greatly simplifies the logistics of evaluating correlation matrices involving large numbers of operators. Implementing the Wick contractions of the quark lines is also straightforward. Contributions from different Wick orderings within a class of quark-line diagrams differ only by permutations of the noises at the source.

The method was tested using the isoscalar mesons in the scalar, pseudoscalar, and vector channels, and using the two-pion system of total isospin $I = 0, 1, 2$ on large anisotropic $24^3 \times 128$ lattices with pion masses $m_\pi \approx 390$ and 240 MeV. Given the success of these tests, we are now applying the stochastic LapH method to compute the excitation spectrum of both mesonic and baryonic stationary-states of QCD in large finite volume.

Acknowledgments

This work was supported by the U.S. National Science Foundation under awards PHY-0510020, PHY-0653315, PHY-0704171, PHY-0969863, and PHY-0970137, and through TeraGrid resources provided by the Pittsburgh Supercomputer Center, the Texas Advanced Computing Center, and the National Institute for Computational Sciences under grant numbers TG-PHY100027 and TG-MCA075017. MP is supported by Science Foundation Ireland under research grant 07/RFP/PHYF168. We acknowledge conversations with Balint Joo, Steve Wallace, David Richards, Robert Edwards, Jozef Dudek, Christopher Thomas, and Huey-Wen Lin. The USQCD QDP++/Chroma library[27] was used in developing the software for the calculations reported here.

[1] B. S. DeWitt, Phys. Rev. **103**, 1565 (1956).
[2] U. J. Wiese, Nucl. Phys. Proc. Suppl. **9**, 609 (1989).
[3] M. Luscher, Nucl. Phys. **B364**, 237 (1991).
[4] K. Rummukainen and S. A. Gottlieb, Nucl. Phys. **B450**, 397 (1995).
[5] S. Basak, R. Edwards, G. Fleming, U. Heller, C. Morningstar, D. Richards, I. Sato, and S. Wallace, Phys. Rev. D **72**, 094506 (2005).
[6] S. Basak, R. Edwards, G. Fleming, U. Heller, C. Morningstar, D. Richards, I. Sato, and S. Wallace, Phys. Rev.

D **72**, 074501 (2005).
[7] S. Basak, R. Edwards, G. Fleming, K. Juge, A. Lichtl, C. Morningstar, D. Richards, I. Sato, and S. Wallace, Phys. Rev. D **76**, 074504 (2007).
[8] J. Bulava et al., Phys. Rev. D **79**, 034505 (2009).
[9] C. Morningstar et al., AIP Conf. Proc. **1257**, 779 (2010), arXiv:1002.0818 [hep-lat].
[10] J. Dudek, R. Edwards, M. Peardon, D. Richards, and C. Thomas, Phys. Rev. Lett. **103**, 262001 (2009).
[11] M. Mahbub, A. Cais, W. Kamleh, B. Lasscock, D. Leinweber, and A. Williams, Phys. Rev. D **80**, 054507 (2009).
[12] M. S. Mahbub, A. O. Cais, W. Kamleh, D. B. Leinweber, and A. G. Williams, Phys. Rev. **D82**, 094504 (2010).
[13] G. P. Engel, C. B. Lang, M. Limmer, D. Mohler, and A. Schafer, Phys. Rev. **D82**, 034505 (2010).
[14] J. Bulava et al., Phys. Rev. D **82**, 014507 (2010).
[15] J. J. Dudek et al. (2011), arXiv:1102.4299 [hep-lat].
[16] C. Michael, Nucl. Phys. **B259**, 58 (1985).
[17] M. Luscher and U. Wolff, Nucl. Phys. **B339**, 222 (1990).
[18] M. Peardon et al., Phys. Rev. **D80**, 054506 (2009).
[19] J. Foley et al. (2010), arXiv:1011.0481 [hep-lat].
[20] J. Bulava et al., PoS **(LAT2010)**, 110 (2010).
[21] C. Morningstar and M. J. Peardon, Phys. Rev. **D69**, 054501 (2004).
[22] J. Foley, K. J. Juge, A. O'Cais, M. Peardon, and S. M. Ryan, Comput. Phys. Commun. **172**, 145 (2005).
[23] S. Bernardson, P. McCarty, and C. Thron, Comput. Phys. Commun. **78**, 256 (1993).
[24] W. Wilcox (1999), hep-lat/9911013.
[25] R. G. Edwards, G. Fleming, B. Joo, K. Juge, A. Lichtl, C. Morningstar, D. Richards, and S. Wallace, PoS **(LAT2007)**, 108 (2007).
[26] J. Bulava, R. Edwards, K. J. Juge, C. J. Morningstar, and M. J. Peardon, PoS **(LAT2008)**, 100 (2008).
[27] R. G. Edwards and B. Joo (SciDAC), Nucl. Phys. Proc. Suppl. **140**, 832 (2005).
[28] K. Wu and H. Simon, SIAM. J. Matrix Anal. & Appl. **22**, 602 (2000).
[29] H. Rutishauser, *Description of Algol 60: Handbook for Automatic Computation* (Springer Verlag, Berlin, 1967).
[30] K. Wu and H. Simon, Lawrence Berkeley National Laboratory Technical Report LBNL-42982 (1999).
[31] H.-W. Lin et al. (Hadron Spectrum), Phys. Rev. **D79**, 034502 (2009).
[32] M. A. Clark, A. D. Kennedy, and Z. Sroczynski, Nucl. Phys. B (Proc. Suppl.) **140**, 835 (2005).
[33] S. Duane, A. D. Kennedy, B. J. Pendleton, and D. Roweth, Phys. Lett. **B195**, 216 (1987).
[34] R. Brower, S. Chandrasekharan, J. W. Negele, and U. J. Wiese, Phys. Lett. **B560**, 64 (2003).
[35] S. Aoki, H. Fukaya, S. Hashimoto, and T. Onogi, Phys. Rev. **D76**, 054508 (2007).